

NASA Contractor Report 4715

IN-71
44506

Aeroacoustic Analysis of Turbofan Noise Generation

Harold D. Meyer and Edmane Envia

CONTRACT NAS3-26618 and NAS3-27186
MARCH 1996



National Aeronautics and
Space Administration

NASA Contractor Report 4715

Aeroacoustic Analysis of Turbofan Noise Generation

Harold D. Meyer
*United Technologies Corporation
Hamilton Standard Division
Windsor Locks, Connecticut*

and

Edmane Envia
*NYMA, Inc.
Brook Park, Ohio*

Prepared for
Lewis Research Center
under Contract NAS3-26618 and NAS3-27186



National Aeronautics and
Space Administration

Office of Management

Scientific and Technical
Information Program

1996

TABLE OF CONTENTS

	Page
LIST OF SYMBOLS	iv
LIST OF FIGURES	viii
SUMMARY	ix
CHAPTER 1: INTRODUCTION	1
1.1 Background	1
1.2 Overview	2
CHAPTER 2: GEOMETRY OF DUCT, ROTOR AND STATOR	7
CHAPTER 3: MEAN ROTOR WAKE	12
3.1 Rotor Wake Model	12
3.2 Stator Upwash Velocity	16
3.3 Loading on Stator Vanes	18
CHAPTER 4: DUCT ACOUSTICS	21
4.1 Normal Modes in an Annular Duct	21
4.2 Duct Acoustic Modes	25
4.3 Sound Power	31
CHAPTER 5: NON-DIMENSIONAL RESULTS	32
5.1 Pressure Amplitude	32
5.2 Sound Power	35
CHAPTER 6: CONCLUDING REMARKS	37

APPENDIX A: KERNEL FUNCTION FOR A LINEAR CASCADE
IN SUBSONIC FLOW 38

APPENDIX B: NUMERICAL COMPUTATION OF THE NORMAL MODES
IN AN ANNULAR DUCT 48

APPENDIX C: SOUND POWER FLUX 50

APPENDIX D: FILON'S INTEGRATION RULE 54

APPENDIX E: NUMERICAL SOLUTION OF THE INTEGRAL EQUATION
FOR THE VANE LOADING 56

REFERENCES 59

ACKNOWLEDGEMENTS 61

LIST OF SYMBOLS

A_{mns}	duct mode amplitude
B	rotor blade count
b	vane semi-chord
b_T	vane semi-chord at the tip
\bar{b}	$b/2b_T$
$C_{mns}(x)$	chordwise integral of elemental vane loading
$\hat{c} = (\cos \alpha_s, -\sin \alpha_s)$	unit vector along vane chord
c_0	medium nominal speed of sound
$\vec{D} = (D_1, D_2)$	blade trailing edge to vane leading edge distance in (X_1, X_2) coordinates
\hat{e}_1	unit vector along X_1 (i.e., axial direction)
\hat{e}_2	unit vector along X_2 (i.e., azimuthal direction)
$F = f \sin \psi$	“reduced” (non-singular) elemental vane loading function
f	elemental vane loading function
f_s	s th Fourier harmonic of f
$G(\vec{x}, \vec{y})$	Green’s function
H	blade spacing
H_1	chordwise component of H
H_2	transverse component of H
h	vane spacing
h_1	chordwise component of h
h_2	transverse component of h
I_{ax}	axial component of acoustic energy flux vector
$\langle I_{ax} \rangle$	acoustic intensity (i.e., time-averaged I_{ax})
i	$\sqrt{-1}$
$J_m(\cdot)$	m th order Bessel function of the first kind
K	reduced frequency
$K_c(\cdot)$	cascade kernel function

k_s	chordwise gust wavenumber
\tilde{k}_s	$k_s b$
k_{mns}	axial wavenumber of duct mode relative to the flow
\tilde{k}_{mns}	$k_{mns} r_D$
M	duct uniform axial velocity Mach number (used for acoustic calculations)
M_r	Mach number of stator relative flow
M_T	rotor blade tip rotational Mach number
$m = sB - qV$	circumferential wavenumber of acoustic duct mode
\hat{N}	unit normal to blade (mean) surface
\vec{n}	unit outward normal to vane surface
\hat{n}	unit normal to vane (mean) surface
n	duct radial mode index
p	acoustic pressure
p_{mns}	complex harmonic duct mode pressure amplitude
\bar{p}	Fourier transform of p
p_s	sth Fourier harmonic of p
p_s^+	p_s on the vane upper surface
p_s^-	p_s on the vane lower surface
$r = \sqrt{x_2^2 + x_3^2}$	radial coordinate
r_D	duct outer radius
r_H	duct inner radius
$S(\vec{y})$	vane surface (both upper and lower)
S_M	vane mean surface
S_0	mean surface of reference vane
s	BPF harmonic index
t	time variable
\vec{U}_r	velocity relative to the stator
U	duct uniform axial velocity (used for acoustic calculations)
u	acoustic axial velocity
V	vane count

$\vec{W} = (W_1, W_2)$	wake velocity downstream of the rotor
W_s	Fourier coefficient of W
\hat{w}	unit vector along \vec{W}
$w = (w_1, w_2)$	stator upwash
w_s	Fourier coefficient of w
\tilde{w}_s	w_s/U_r
$\vec{X} = (X_1, X_2)$	2-D coordinate system fixed to the rotor trailing edge (cartesian system)
$X_{mn} = \kappa_{mn} r_D$	duct mode radial eigenvalue (non-dimensional)
$\vec{x} = (x_1, x_2, x_3)$	coordinate system fixed to the stator leading edge (cartesian system)
$\vec{x} = (r, \phi, x_1)$	coordinate system fixed to the stator leading edge (cylindrical polar system)
x	r/r_D (Chapter 5 only)
x_{SD}	axial displacement of vane leading edge
x_S	$x_{SD}/2b_T$
x_{SOR}	$x_{SPAC}/2b_T$
x_{SPAC}	blade trailing edge to vane leading edge axial distance
$Y_m(\cdot)$	m th order Bessel function of the second kind
$\vec{y} = (y_1, y_2, y_3)$	source coordinates (cartesian)
$\vec{y} = (r', \phi', y_1)$	integration point (cylindrical)
y_{RD}	azimuthal displacement of rotor trailing edge
y_R	$y_{RD}/2b_T$
y_{SD}	azimuthal displacement of vane leading edge
y_S	$y_{SD}/2b_T$
z	chordwise coordinate along the vane
α	Fourier transform variable (for y_1)
α_{CL}	blade relative velocity flow angle
α_s	vane stagger angle
β	$\sqrt{1 - M^2}$

β_r	$\sqrt{1 - M_r^2}$
Γ	$\pi(r_D^2 - r_H^2)$ (Chapter 4)
Γ	$\sigma - \alpha b h_1 - K h_1 / M_r$ (Appendix A)
Γ_n	$\Gamma - 2n\pi$ (Appendix A)
γ_{mns}	axial wavenumber of duct mode in stator-fixed frame
$\tilde{\gamma}_{mns}$	$\gamma_{mns} r_D$
$\Delta p_s = p_s^- - p_s^+$	vane unsteady loading
Δp_ν	unsteady loading on the ν th vane
$\Delta p_{\nu,s}$	s t h Fourier coefficient of Δp_ν
θ	z/b chordwise transformed variable (collocation point)
κ_{mn}	duct mode radial eigenvalue (dimensional)
λ	wavenumber in the Fourier transformed plane (Appendix A)
ν	vane index
ρ_0	nominal fluid density
σ	inter-blade phase angle
σ_c	$2b_T / r_D$
σ_r	r_H / r_D
$\phi = \tan^{-1} \frac{x_3}{x_2}$	polar (angle) coordinate
χ_p	period used in definition of Fourier series
ψ	chordwise transformed variable (integration point)
$\psi_m(\kappa_{mn} r)$	duct radial mode
Ω	fan rotational speed

LIST OF FIGURES

	Page
Figure 2.1. Sketch of Rotor/Stator Combination.	8
Figure 2.2. Blade and Vane Geometry.	9
Figure 2.3. Rotor/Stator “Unrolled” Geometry.	11
Figure 3.1. Rotor/Stator Geometry for Mean Wake Analysis Shown at Time $t = 0$	13
Figure 4.1. Stator Geometry for Acoustic Mode Analysis.	27
Figure A.1. Stator Cascade Geometry.	39
Figure A.2. Integration Contour for Eq. (A.30).	45

SUMMARY

This report provides an updated version of analytical documentation for the *V072 Rotor Wake/Stator Interaction Code*. It presents the theoretical derivation of the equations used in the code and, where necessary, it documents the enhancements and changes made to the original code since its first release.

V072 is a package of *FORTRAN* computer programs which calculate the in-duct acoustic modes excited by a fan/stator stage operating in a subsonic mean flow. Sound is generated by the stator vanes interacting with the mean wakes of the rotor blades. In this updated version, only the tonal noise produced at the blade passing frequency and its harmonics, is described. The broadband noise component analysis, which was part of the original report, is not included here. The code provides outputs of modal pressure and power amplitudes generated by the rotor-wake/stator interaction.

The rotor/stator stage is modeled as an ensemble of blades and vanes of zero camber and thickness enclosed within an infinite hard-walled annular duct. The acoustic pressure within the duct is calculated by distributing pressure dipoles on the surface of the stator vanes and calculating the pressure at an arbitrary point within the duct via the normal mode expansion of the Green's function for an annular duct. By this procedure one obtains an infinite series for the sound pressure within the duct. Each term contains a normal mode of the duct multiplied by the amplitude of that mode. The amplitude of each propagating mode is computed and summed, with appropriate factors, to obtain the harmonics of sound power flux within the duct. These calculations are carried through for both upstream and downstream propagating modes.

No assumptions regarding the ratio of the wavelength of the sound generated to the vane chord are required. However, to simplify the computation of the dipole distribution generated by a given periodic inflow variation, the so-called strip theory approximation is employed. Specifically, the dipole distribution is computed by deleting, from the convected wave equation, all terms containing derivatives with respect to radius, but retaining the radius as a parameter in the boundary conditions (which derive from the vane geometry and the incident fluid flow). At each radius, therefore, the equations to be solved are

those for a linear cascade in subsonic flow. Although radial derivatives are deleted from the wave equation in calculating the chordwise pressure distribution on the vanes, radial variations in the amplitude and phase of the pressure distribution are taken into account in integrating over the vane surface to obtain the amplitudes of the propagating duct modes.

The wake flow downstream of the rotor is modeled as a small amplitude disturbance flow, superimposed upon a steady mean flow. The mean part of the flow is assumed to have no radial component, so that the mean flow stream surfaces are cylindrical. It is further assumed that if one of these cylinders is unwrapped to form a plane, the mean flow streamlines will be parallel. This is equivalent to ignoring viscous diffusion in the rotor wakes, a justifiable approximation as regards the calculation of the forces on the stator vanes, provided that the wake thickness chosen is that which is obtained at the axial station of the stator vanes themselves. The magnitude of the wake flow velocity is constant on lines parallel to the mean flow streamlines, but varies periodically in the direction normal to the mean flow streamlines.

CHAPTER 1

INTRODUCTION

1.1 Background

This report is a revision of the original analytical documentation for a rotor-wake/ stator interaction computer code described in NASA contractor report, CR-167952. The code, which was originally developed under contract to NASA by Bolt Beranek and Newman Inc., was later revised and integrated into a fan noise prediction system by Pratt & Whitney and renamed the *v072* code. This report replaces Volume 1 of the original two-volume documentation authored by Ventres et al.¹ Volume 2, "Computer Programs," of the same set² is superseded by a revised technical documentation and user's manual written by Topol and Mathews.³ The current revision, while primarily a mathematical treatment, should also enable a diligent reader to trace through the actual computer code without the need for the old Volume 2.

This revision was necessary for several reasons. First, and most important, because the original documentation preceded the actual release of the computer program, it did not reflect many of the changes to the code. In particular, the geometry used for the code, and, as a consequence, the resulting coded formulae, are different from those described in the old Volume 1. Second, the original report covered, in addition to discrete-tone noise sources produced by mean rotor wakes, broadband noise sources due to turbulent rotor wakes. These broadband noise capabilities are included in other codes but are not part of the *v072* computer program. Finally, there have been several undocumented corrections and enhancements to the code since it was first released.

Outside of the changes described above, most of the material in this revision has been borrowed intact from the original documentation, although some of it has been rearranged to improve the flow of the text. Where necessary, complete sections have been deleted from the material. These include all of the discussion on broadband noise sources which, as mentioned earlier, is not included in the computer program. These sections cover modeling of the rotor turbulent wakes and their attendant acoustic response computations (i.e., broadband noise spectrum and acoustic power). Therefore, with no further need for

a general frequency treatment, all of the material in this revision is rewritten in terms of discrete harmonics of the rotor blade passing frequency.

1.2 Overview

Given a description of the rotor and stator geometries and their operating conditions, the *V072* code calculates the modal content of the acoustic fields set up inside the inlet and exhaust ducts of a turbofan by the actions of unsteady vortical velocity fluctuations convected past the stator vanes. The results from this code, supplemented by mathematical models of the impedance of the inlet and exhaust terminations, or coupled with stand-alone radiation codes such as the one developed by Eversman,⁴ can be used to calculate the farfield noise. The program can also be used to provide the initial conditions required for the investigation of duct liners, particularly liners tailored to suppress a specific mode or set of modes.

In the context of discrete rotor/stator interaction noise, the fluctuating velocity field, i.e., vortical flow, is caused by the periodic wakes of the upstream blade row of a fan operating in front of an outlet guide vane. The fluctuations are assumed to be small enough so as to be convected by the mean flow. When these velocity fluctuations are carried past the rigid surface of a stator vane, the requirement of flow tangency sets up acoustic pressure fluctuations, which propagate upstream and downstream in the duct, and are perceived as noise.

The acoustic pressure in the duct can be calculated in a straightforward manner using the Green's function for the duct, provided that the pressure distributions on the surface of the stator vanes are known. If the Green's function is expressed as an infinite series of the normal modes of the duct, the modal amplitudes of the acoustic pressure field are obtained directly. The problem remaining, therefore, is to determine the pressure distributions on the surface of the stator vanes generated by the convected vortical flow. This is accomplished by modeling the vanes as surfaces of zero thickness and camber, which support an unknown but continuous distribution of pressure dipoles. The normal velocity on the vanes induced by the unknown dipole distribution is then required to nullify the normal component of the vortical disturbance velocity so that the total fluid velocity conforms to the shape of the blades. The result is an integral equation for the

dipole distribution, which, depending upon the approximations introduced, may admit an analytic solution, or may require numerical treatment.

The approximations required to arrive at an analytic solution are considerable; essentially they ignore the annular or circular geometry of the fan, or stator, the three-dimensionality of the disturbance, the interaction between the blades, and the compressibility of the fluid. What remains is incompressible flow around an isolated airfoil in two dimensions, the solution of which, for a sinusoidal vortical gust, is known as the Sears function. This was the approach used by Kemp and Sears^{5,6} in their original investigations of the interactions between blade rows in axial flow turbomachinery. The incompressible approximation has since been shown to be unacceptable. For example, Fleeter⁷ found that compressibility can change the pressure values on the rotor or stator by as much as a factor of two, while Kaji⁸ calculated even greater changes (20 dB; a factor of 10) in the sound pressure level upstream of the blade row due to source non-compactness.

At the opposite extreme, as regards complexity, are calculations carried out by Kobayashi⁹ and Kobayashi and Groeneweg¹⁰, using equations derived by Namba^{11,12} for an annular blade row in compressible flow. Because of the annular geometry, the kernel function, which relates the dipole distribution to the velocity normal to the blades, is elaborate in form and time-consuming to compute. The associated integral equation is two-dimensional (i.e., both the spanwise and chordwise distributions of pressure dipoles must be determined). In his numerical work, Kobayashi made comparisons between “exact” aerodynamic theory and various approximate methods of calculating the normal component of the induced velocity. One of these, which he called the “quasi-three-dimensional” approximation, coincides with what most would call a “strip theory” approximation. In calculating the induced velocity, derivatives with respect to radius are deleted from the convected wave equation, so that one is left with the kernel function of a linear cascade in unsteady compressible flow. The particular geometry of the cascade, as well as the vortical inflow velocity, depend on the radius, and this parametric dependence is retained in calculating the induced velocity and, hence, ultimately the dipole distribution. The effects of radial or spanwise variations in the amplitude and phase of the vortical disturbance velocity, as well as radial variations in blade chord, inter-blade gap, and stagger angle, are thereby taken into account, even if in an approximate manner. Kobayashi found that

this procedure introduced errors no greater than 2 dB in the computed magnitudes of the acoustic modes set up in the duct upstream and downstream of the rotor. Furthermore the strip theory approximation, as described above, is considerably easier than the “exact” method to implement numerically. For these reasons, this approximation was selected for use in the V072 program.

Lakshminarayana et al.¹³⁻¹⁵ have collected an extensive set of measurements of the mean and fluctuating components of the flow downstream of a multi-bladed fan operating at subsonic tip speed, using a transducer rotating at the same rate as the fan. Their measurements of the mean, or time-averaged, component of the flow at locations remote from the blade hub or tip indicate that the radial velocity immediately downstream of the fan blade trailing edges is substantial, but that this velocity decays rapidly, so that at distances greater than about one-half blade chord downstream the circumferential and axial components of the mean velocity predominate. Measurements of the velocity defect profile for each fan blade show marked asymmetry about the streamlines on which the minimum velocity occurs, but this asymmetry also disappears within a half-chord length downstream of the fan blade trailing edges. At greater distances, the normalized velocity defect profiles all show a Gaussian distribution.* Due to the diffusion of momentum in the flow, the widths of the velocity defect profiles increase with downstream distance, while the maximum velocity defect decreases. But for the purpose of calculating the noise radiated by the stator, it is sufficient to model the wake flow in the vicinity of the stator. This can be done by ignoring momentum diffusion between the fan and stator, provided that the wake thickness and velocity defect are assigned the values they attain in the vicinity of the stator, say at the leading edges of the stator vanes.

With these approximations, the mean flow streamlines downstream of the fan become a series of parallel lines, as viewed on a cylindrical surface opened out to form a plane. On this plane the velocity defect profile of each rotor blade is assumed to be a Gaussian wake profile, with wake width and maximum velocity defect left as parameters to be

* Since the original version of the code was released, hyperbolic¹⁶ and loaded rotor¹⁷ wake profiles, which are more representative of modern fans, have also been added. The loaded rotor model, in particular, indicates that asymmetric profiles may have a non-negligible influence on the predicted noise levels.

specified. When viewed in a stationary frame of reference fixed to the stator, the pattern, which is spatially periodic, becomes a temporally periodic fluctuation which can most conveniently be expressed in terms of a Fourier series for the purpose of calculating the inflow disturbances normal to the stator vanes. Further details of the implementation of the wake model in the code will be given in Chapter 3.

One additional aspect of the mean wake geometry is noteworthy. At each radius the mean flow streamlines all bear the same angle to the centerline of the duct, but this angle is a function of the radius, the precise nature of which depends upon the radial variation of the rotor loading. The locus of centerlines of any given wake form a surface whose shape depends upon the radial variation of the wake angle; this surface will normally intersect any selected stator vane at only one point, and this point will move along the leading edge of the stator vane as the fan rotates. If the gap between the fan and stator is large, each stator vane will at any given instant intersect many rotor blade wakes, and, for each wake intersected, there will be two changes in the sign of the disturbance velocity seen by the stator vane. The pressure induced on the stator vane will have as many sign reversals as the inflow velocity, and will tend to excite duct acoustic modes with that same number of radial nodes. If, at the frequency of interest (which, of course, must be the blade passage frequency or one of its harmonics), few or none of the duct modes with that number of radial nodes propagate in the duct, the stator will not, at that frequency, be an effective generator of sound. The significance of this wake roll-up phenomenon in the generation of sound by the stator was pointed out previously by Bliss, et al.¹⁸ In their discussion, they chose to emphasize the radial trace velocity of the vane/wake intercept instead of the number of nodes in the normal component of the inflow velocity. Their criterion for efficient sound generation, namely that the trace velocity of the points of intersection of the wake centerlines with the stator vanes be supersonic, is perhaps more appropriate to an unshrouded rotor/stator combination, but the two criteria are roughly equivalent when the ratio of hub and tip radii is close to one, and are exactly equivalent for a set of two linear cascades in relative motion between two infinite parallel planes.

In the equations derived in this report, and in the computer program developed from them, the radial variation of the angle between the mean wake streamlines and the duct centerline may be specified arbitrarily, so that the effects of wake roll-up are properly taken

into account.

One element of the program, which was absent in the original version, is a model for rotor hub and tip vortex flowfields. The details of the model may be found in Ref. 16, where measured rotor flow data were used to develop empirical relations for the vortex flowfield. While the model may not be sufficiently robust to allow for realistic calculations of the vortex noise contribution, it does enable one to perform a parametric assessment of the potential impact of a tip, or hub, vortex on the rotor/stator interaction noise.

The remainder of the report is organized as follows. Pertinent aspects of the duct, rotor and stator geometries are discussed in Chapter 2. Mathematical models of the fan blade mean wake and its hub and tip vortex flows, which together represent the rotor gust upwash, are presented in Chapter 3. The chapter then concludes with a discussion of the computation of the stator vane pressure distribution generated in response to the gust upwash. An overview of the acoustics of annular ducts is given in Chapter 4, along with a derivation of the amplitudes of the duct modes excited by stator vane pressure distributions. The expression for the acoustic power in the duct is also presented. Chapter 5 presents key formulae for duct mode amplitudes and acoustic power derived in earlier chapters in non-dimensional forms corresponding to those used in the code. Details on cascade response and numerical methods are given in Appendices A through E.

CHAPTER 2

GEOMETRY OF DUCT, ROTOR AND STATOR

For our purposes, a turbofan is a rotor and stator combination mounted in an annular duct of infinite length (i.e., reflection of acoustic waves from the ends of the duct are ignored). A sketch of the rotor/stator combination is shown in Fig. 2.1. As shown in the figure, a cylindrical polar coordinate system is established in the duct, with the polar axis lying along the duct centerline. The axial coordinate x_1 , increases in the direction of the air flow, and the rotor rotates in the sense of increasing ϕ with fan rotational speed Ω . Note that the meaning for x_1 , x_2 and x_3 in subsequent figures is sometimes different from that in Fig. 2.1. The outer radius of the duct is r_D and the inner radius is r_H . The rotor has B identical evenly spaced blades and the stator has V identical evenly spaced vanes. This is the same coordinate setup as used in Ref. 19, page 190, from which we later obtain our Green's function.

The rotor blades and stator vanes are modeled as twisted sheets of zero thickness and camber, whose stagger and chord vary with the radius, r . The axial and azimuthal sweep, if any, of the stator vanes are defined by extending a radial line from the axis of rotation through the leading edge point of the vane at the hub (radius $r = r_H$). As shown in Fig. 2.2, the location of the leading edge point at any other radius r is defined by the two parameters x_{SD} and y_{SD} which give the displacements of this point from the radial line. (x_{SD} = axial displacement of the stator vane leading edge, y_{SD} = azimuthal displacement of the stator vane leading edge.) Similarly, the azimuthal sweep of the rotor blades is defined by extending a radial line from the axis of rotation through the trailing edge point of the blade at the hub. The location of the trailing edge point at any other radius r is defined by the parameter y_{RD} which gives the displacement of this point from the radial line. (y_{RD} = azimuthal displacement of the rotor trailing edge.*) In general, x_{SD} , y_{SD} and y_{RD} are functions of the radius, and by definition, $x_{SD} = y_{SD} = y_{RD} = 0$ at the hub.

* No axial sweep parameter is used for the rotor. Instead a rotor/stator distance parameter, x_{SPAC} , which represents the axial distance between the rotor trailing edge and the stator leading edge, accounts for any axial sweep that might exist.

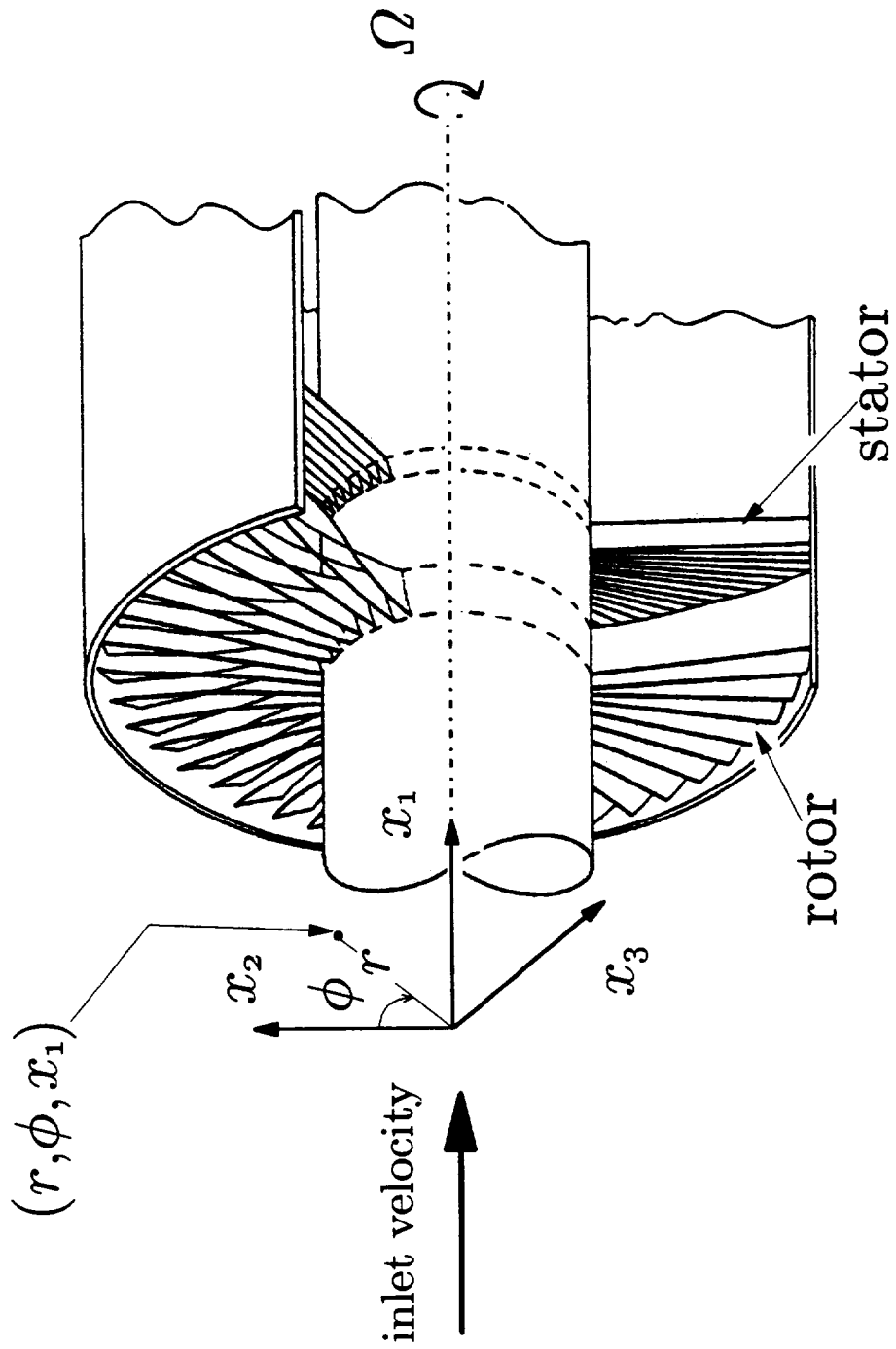
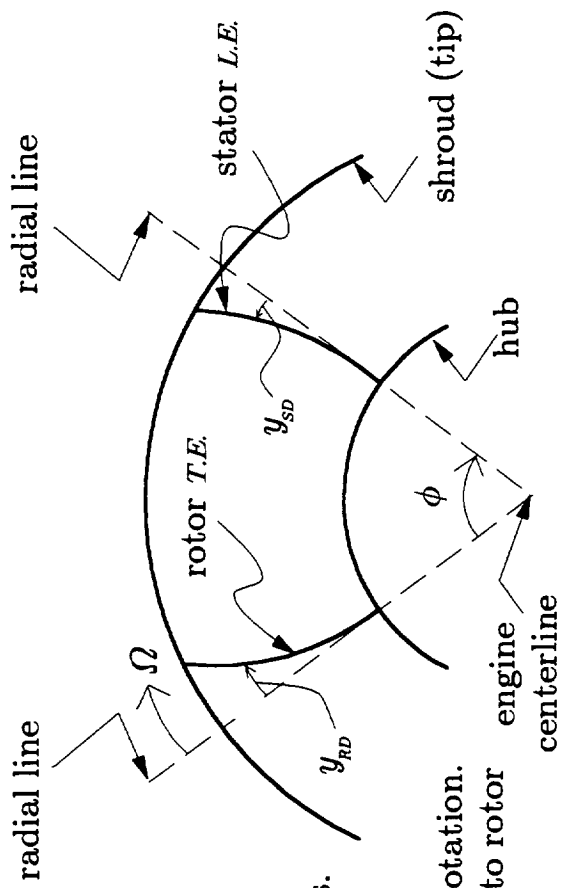


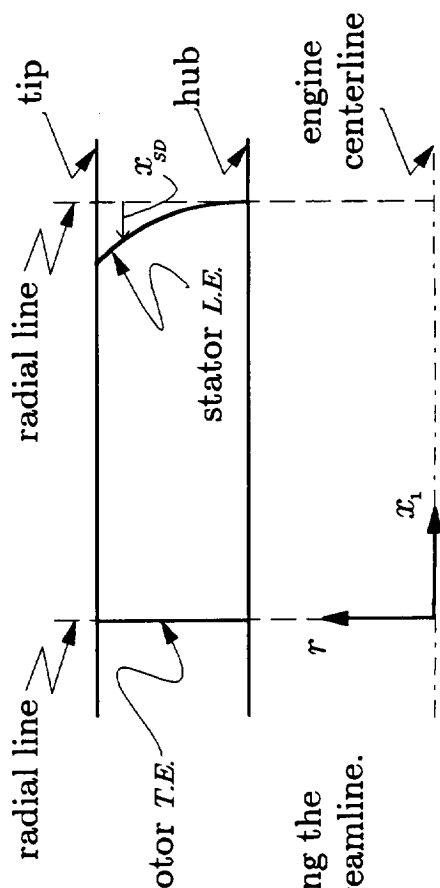
Fig. 2.1 Sketch of Rotor/Stator Combination.



(a) Definition of y_{RD} and y_{SD} :

Schematic view of rotor blade *T.E.* and stator vane *L.E.* looking down the x_1 -axis.

y_{RD} is positive in the direction of rotor rotation.
 y_{SD} is positive in the direction opposite to rotor rotation.



(b) Definition of x_{SD} :

Schematic view of rotor blade *T.E.* and stator vane *L.E.* looking perpendicular to the rotor axis.

x_{SD} is positive in the direction of reducing the axial spacing relative to the hub streamline.

Fig. 2.2 Blade and Vane Geometry.

The intersections of the rotor blades and stator vanes with a cylindrical surface of radius r is shown in Fig. 2.3. This is for the point in time where the rotor trailing edge and stator leading edge are aligned azimuthally at the hub. The stagger angle of the vanes is α_s . The spacing between the blades is $2\pi r/B$, and between the vanes, $2\pi r/V$. The local semi-chord of the vanes is b which can be a function of r .

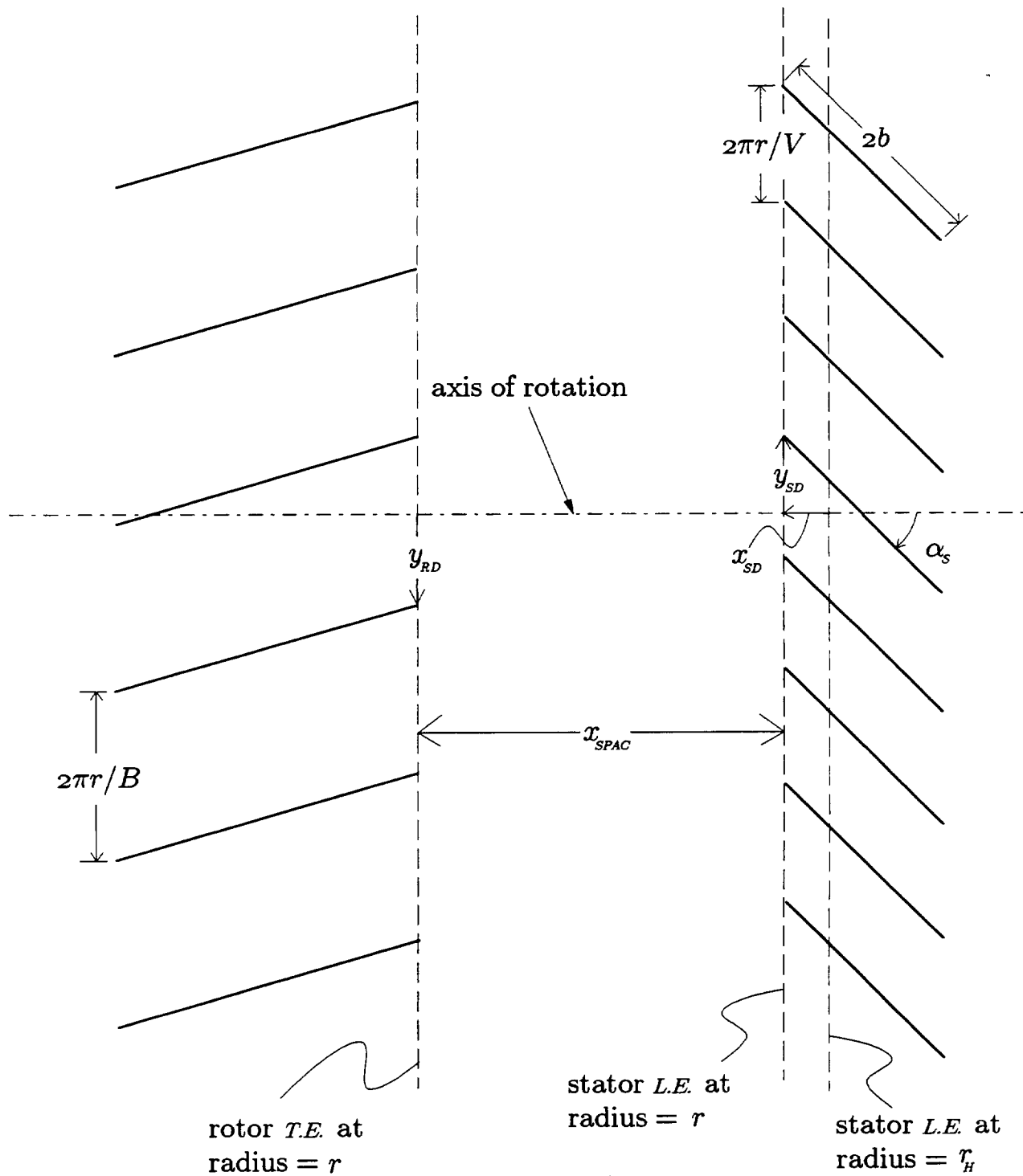


Fig. 2.3 Rotor/Stator "Unrolled" Geometry.

CHAPTER 3

MEAN ROTOR WAKE

In this chapter, we provide information that will be needed for computing the acoustic response discussed later in Chapter 4. Our basic geometry will be a constant-area annular duct, through which a uniform flow is assumed. We shall describe a rotor wake model from which we derive an expression for the wake velocity normal to the stator vanes; from this expression we obtain the unsteady loading along the stator vanes. The loading will then be used in Chapter 4 to derive an expression for the complex amplitudes of the duct modes excited by the interaction of the rotor blade wakes with the stator vanes. These amplitudes will in turn give us the power propagating up and down the duct.

3.1 Rotor Wake Model

The pressure distribution on the stator vanes can be calculated by dividing the stator into a series of radial “strips” at constant radius and calculating the pressure on each “strip” as though it were a linear cascade of thin flat plates. In this approximation, the radial variation of the inflow to the vanes is ignored - - an application of “strip theory” to stator aerodynamics. We are concerned here only with the mean value (time average in rotor coordinates) of the rotor wakes, which, being time periodic in stator coordinates, generate sound at harmonics of the blade passage frequency $\Omega B/2\pi$.

Consider a cylinder of radius r , centered on the duct’s axis of symmetry. The intersection of this cylinder with the rotor and stator is depicted in Fig. 3.1. This surface is the one viewed by looking down the positive x_3 -axis in Fig. 2.1 toward the origin. In Fig. 3.1, two sets of coordinate axes are shown; axes (X_1, X_2) are fixed at the trailing edge of the rotor, while axes (x_1, x_2) are fixed at the leading edge of the stator. The azimuthal coordinate, $(r\phi)$, is in the opposite direction to the x_2 -axis as indicated in the figure. Rotor rotational speed, $r\Omega$, is in this same direction. The (x_1, x_2) -coordinate system is defined at each radius and places the leading-edge points of the stator vanes at the points $(0, -\nu h)$, where ν is any integer and $h = 2\pi r/V$. As seen in the figure, ν increases in the direction of increasing x_2 (decreasing ϕ).

The relation between the two sets of axes in Fig. 3.1 is

$$\vec{X} = \vec{x} + \vec{D} + \Omega r t \hat{e}_2, \quad (3.1)$$

where \hat{e}_2 is the unit vector in the azimuthal direction and $\vec{D} = \vec{D}(\vec{r})$ is the vector distance from the trailing edge of a rotor blade to the leading edge of a stator vane. \vec{D} is shown for the case where, at $t = 0$, the trailing edge of the rotor is aligned azimuthally with the leading edge of the stator at the hub (i.e., $r = r_H$). We will perform our initial analysis based on this configuration. However, \vec{D} actually is defined only to within an additive vector $r\phi_0\hat{e}_2$, where ϕ_0 represents an arbitrary angle of rotation of the rotor. We shall later indicate the effect of such a ϕ_0 and assign it a particular value.

In Fig. 3.1, \vec{W} , which we will call the wake velocity downstream of the rotor, represents the entire air flow, including the mean flow, downstream of the rotor and in the rotor reference frame. The parameter α_{CL} is the angle that the wake velocity \vec{W} makes with the X_1 -direction at the stator leading edge.

So as to arrive at a reasonably simple model of the rotor wake, which will be valid in the vicinity of the stator vanes, it is convenient to introduce two plausible assumptions. They are

1. no radial flow occurs, and
2. pressure gradients and turbulent and viscous diffusion can be neglected over the chord of the stator.

A result of the second assumption is that the wakes do not change during convection across the stator. The fluid velocity then has only two components, (W_1, W_2) in (X_1, X_2) coordinates, and the equations of motion of the fluid reduce to

$$(\vec{W} \cdot \nabla) \vec{W} = 0, \quad (3.2)$$

$$\nabla \cdot (\rho_0 \vec{W}) = 0, \quad (3.3)$$

where ρ_0 is the nominal fluid density. A parallel flow of the form

$$\vec{W} = W(\vec{X} \cdot \hat{N}) \hat{w}, \quad (3.4)$$

where \hat{N} and \hat{w} are constant orthogonal unit vectors (see Fig. 3.1), is a solution to these equations, and is the form we will assume for the wake. The velocity is everywhere parallel to the unit vector $\hat{w} = (\cos \alpha_{CL}, \sin \alpha_{CL})$, and is constant in magnitude on the lines $\vec{X} \cdot \hat{N} = \text{constant}$. The variation of the magnitude across the wakes is determined by the as-yet-unspecified function $W(\vec{X} \cdot \hat{N})$.

In this report, our Fourier series are defined in terms of the pair

$$f(\chi) = \sum_{s=-\infty}^{\infty} f_s e^{2\pi i s \chi / \chi_p}, \quad (3.5)$$

$$f_s = \frac{1}{\chi_p} \int_{-\chi_p/2}^{\chi_p/2} f(\chi) e^{-2\pi i s \chi / \chi_p} d\chi, \quad (3.6)$$

where χ_p is the period. Let H be the gap between rotor blades, measured azimuthally. Now, $W(\vec{X} \cdot \hat{N})$ is periodic in the \hat{N} direction, because all the wakes are assumed to be identical. The period here is the normal distance between wake centerlines, $\chi_p = H \cos \alpha_{CL}$. $W(\vec{X} \cdot \hat{N})$ can therefore be written as a Fourier series, i.e.,

$$W(\vec{X} \cdot \hat{N}) = \sum_{s=-\infty}^{\infty} W_s e^{i[sB\vec{X} \cdot \hat{N} / (r \cos \alpha_{CL})]}, \quad (3.7)$$

where we have substituted $2\pi r/B$ for H . The unit vector \hat{N} has components $(-\sin \alpha_{CL}, \cos \alpha_{CL})$, so the Fourier series may also be cast in the following form,

$$W = \sum_{s=-\infty}^{\infty} W_s e^{i[sB(X_2 - X_1 \tan \alpha_{CL}) / \tau]}, \quad (3.8)$$

which indicates that the rotor wake velocity is periodic in the azimuthal direction also (as well as the direction normal to the wakes). The azimuthal period is, of course, $2\pi r/B$.

In principle, the Fourier coefficients W_s of the wake flow could be determined experimentally by processing a sufficient number of flow measurements collected from a transducer mounted behind the rotor. If only the first few harmonics of the blade passage

frequency are of interest (it will transpire that the s th harmonic in the wake flow interacts with the stator to generate sound in the s th harmonic of the blade passage frequency), this is a feasible proposition. However, by assuming an explicit (and plausible) form for the wake velocity profile, it is possible instead to characterize the wake velocity profile semi-empirically by using experimental data to estimate the unknown parameters which appear in these forms. In practice, this data is taken at the stator leading edge; however, it must be referenced back to the rotor trailing edge to be appropriate for Eq. (3.7). In defining the W_s 's using Eq. (3.6), note that χ is zero at the wake centerline for *v072*.*

There are presently three wake velocity profiles to choose from in *v072*: (i) Hyperbolic Secant, (ii) Gaussian, and (iii) Loaded Rotor 67. Three types of wake width and velocity correlations are available for use with these profiles: (i) Loaded Fan Wake Function and two types of (ii) Linear Rational Functions. These options will not be discussed here. For information regarding the wake profile and correlation treatment, the reader is referred to Refs. 16 and 17. In addition to wakes, the current version of *v072* now also contains models for hub and tip vortex flows. These empirical vortex models, which were not part of the original code, were added later to provide a more complete representation of the flow field downstream of the fan. In their current form, however, the vortex models are intended, primarily, as a tool for providing crude estimates of the contribution of vortex flow to the rotor/stator interaction noise. As such, they should only be used in parametric assessments of hub and/or tip vortex noise contributions, not as design tools. When selected, these vortex models are combined with the wake profiles so that both are used in determining the W_s 's multiplied by an additional factor $\sin(\alpha_s + \alpha_{CL})$. This is the quantity that appears later in Eq. (3.18). These vortex models are discussed in Ref. 16.

3.2 Stator Upwash Velocity

We next determine the component of wake upwash velocity perpendicular to the stator vanes, using the combined wake/vortex profile in rotor-fixed coordinates at the rotor

* This is not the case for Ref. 16, where, with the notation here, χ would be $\chi_p/2$ at the wake centerline. This means that the W_s 's used in *v072* differ from those defined in Ref. 16 by a factor of $\exp(is\pi)$.

trailing edge, as given by Eq. (3.8). This upwash is specified in terms of its Fourier series harmonics by using a coordinate transformation to stator-fixed coordinates.

We first calculate the wake velocity relative to the stator vanes,

$$\vec{U}_r = \vec{W} - \Omega r \hat{e}_2 \quad (3.9)$$

and then find the component w of this velocity that is normal to the vanes,

$$w = \vec{U}_r \cdot \hat{n}, \quad (3.10)$$

where \hat{n} is the unit surface normal. Evaluating Eq. (3.10) using Eqs. (3.8), (3.9) and the coordinate transformation (3.1), we find that

$$w = - \sum_{s=-\infty}^{\infty} W_s \sin(\alpha_s + \alpha_{CL}) e^{-i[sB(D_2 - D_1 \tan \alpha_{CL})/r]} \times e^{-i[sB(x_2 - x_1 \tan \alpha_{CL})/r + sB\Omega t]}, \quad (3.11)$$

where the W_s 's are the same as before, except that for $s = 0$, the Ωr part of Eq. (3.9) would be needed in evaluating W_0 .*

On any specific vane, say vane ν , the components of $\vec{x} = (x_1, x_2)$, can be found from

$$\vec{x} = z\hat{c} + \nu\vec{h} + b\hat{c}, \quad (3.12)$$

where $\hat{c} = (\cos \alpha_s, -\sin \alpha_s)$ is a unit vector directed along the vane chords, and $\vec{h} = (0, h)$ is the vector separation between any two neighboring vanes. The coordinate z is equal to $-b$ at the vane leading edges and to $+b$ at the trailing edges. In terms of components, Eq. (3.12) can be written as

$$x_1 = (z + b) \cos \alpha_s, \quad (3.13)$$

$$x_2 = -(z + b) \sin \alpha_s + 2\nu r/V. \quad (3.14)$$

* Note, however, that the $s = 0$ case is not relevant to the work here since it represents the steady part of the vane loading.

Also, substitute for D_1 and D_2 the relations

$$D_1 = x_{SPAC}, \quad (3.15)$$

$$D_2 = y_{RD} + y_{SD}, \quad (3.16)$$

which are easily obtained using Fig. 3.1. Then, Eq. (3.11) gives the result

$$w = - \sum_{s=-\infty}^{\infty} w_s e^{i[k_s z - 2\pi\nu s B/V - sB\Omega t]} \quad (3.17)$$

where

$$w_s = -W_s \sin(\alpha_s + \alpha_{CL}) e^{-i[sB(y_{RD} + y_{SD} - x_{SPAC} \tan \alpha_{CL})/r]} \times e^{i[sBb(\sin \alpha_s + \cos \alpha_s \tan \alpha_{CL})/r]}, \quad (3.18)$$

and

$$k_s = \frac{sB}{r} (\sin \alpha_s + \cos \alpha_s \tan \alpha_{CL}). \quad (3.19)$$

In these equations, the parameters W_s , α_s , α_{CL} , y_{RD} , y_{SD} , x_{SPAC} , and b are all functions of the radius r .

Note that, had \vec{D} in Eq. (3.1) included the additive vector $r\phi_0\hat{e}_2$, we would now multiply the right-hand side of Eq. (3.18) by a factor of $\exp(-isB\phi_0)$. This vector, $\phi_0 = -x_{SPAC,H} \tan \alpha_{CL,H}/r$, is used in V072. Therefore, Eq. (3.18) becomes

$$w_s = -W_s \sin(\alpha_s + \alpha_{CL}) e^{-i[sB(y_{RD} + y_{SD} - x_{SPAC} \tan \alpha_{CL} + x_{SPAC,H} \tan \alpha_{CL,H})/r]} \times e^{i[sBb(\sin \alpha_s + \cos \alpha_s \tan \alpha_{CL})/r]}, \quad (3.20)$$

where the subscript H in Eq. (3.20) refers to the stator leading edge location at the hub. Thus the phase in the circumferential direction is defined such that the exponential part of Eq. (3.20) is unity at the stator leading edge location at the hub.

3.3 Loading on Stator Vanes

Because the vanes are impermeable, they must induce an additional velocity to cancel the normal inflow velocity at the vanes themselves. Thus vane pressure loading is generated

by the negative of w and is found numerically by solving an integral equation. This integral equation is obtained by modifying Eq. (A.21), which is derived in Appendix A. Eq. (A.21) can be written as

$$-\frac{w}{U_r}(x_1 + \nu b h_1, x_2 + \nu b h_2) = e^{i\nu\sigma} \int_{-b}^{+b} K_c(x_1 - y, x_2) \frac{\Delta p_0(y) dy}{\rho_0 U_r^2 b}, \quad (3.21)$$

where w is the upwash evaluated at the point $(x_1 + \nu b h_1, x_2 + \nu b h_2)$. The variables x_1 , x_2 , h_1 and h_2 are defined in Fig. A.1, and ν , ρ_0 and b were defined previously. Parameter σ is the inter-blade phase angle, $-2\pi s B/V$, and K_c is the cascade kernel function, both of which are described in Appendix A. Note that the negative sign for σ is a result of our convention for counting blades. Variable U_r is the nominal fluid velocity in the rotor-fixed coordinate system (see Fig. A.1), and Δp_0 is the pressure loading on vane $\nu = 0$, which has arbitrarily been selected to be the reference vane; Δp_ν would be the loading on an arbitrary vane. From the discussion in Appendix A, it is easily seen that

$$\Delta p_\nu = \Delta p_0 e^{i\nu\sigma} = \Delta p_0 e^{-2i\pi\nu s B/V} \quad (3.22)$$

gives the pressure loading on the ν th vane.

If we restrict ourselves to vane $\nu = 0$ by taking $x_1 = z$ and $x_2 = 0$ in Eq. (3.21), where z is the local chordwise coordinate used before, we find that

$$-w(z, 0) = \int_{-b}^{+b} K_c(z - y, 0) \frac{\Delta p_0(y) dy}{\rho_0 U_r b}. \quad (3.23)$$

If w above is taken only to represent a single harmonic, then we use $w_s \exp(ik_s z)$ (for vane $\nu = 0$) from Eq. (3.17) in its place, and Eq. (3.23) becomes

$$w_s e^{ik_s z} = \int_{-b}^{+b} K_c(z - y) \frac{\Delta p_{0,s}(y) dy}{\rho_0 U_r b}. \quad (3.24)$$

In Eq. (3.24), we have suppressed the 0 in the argument of K_c and replaced Δp_0 with $\Delta p_{0,s}$, where $\Delta p_{0,s}$ is the s th Fourier series harmonic for Δp_0 . Finally, we can write

Eq. (3.24) as

$$e^{ik_s z} = \int_{-b}^{+b} K_c(z-y) f_s(r, y) \frac{dy}{b}, \quad (3.25)$$

if we take

$$f_s(r, z) = \frac{\Delta p_{0,s}}{\rho_0 U_r w_s}. \quad (3.26)$$

In *v072*, we solve Eq. (3.25) for $f_s(r, z)$, the elemental stator vane loading function, to find the vane unsteady pressure loading. Given $f_s(r, z)$, the s th harmonic of the pressure on vane ν , $\Delta p_{\nu,s}$, is given by

$$\Delta p_{\nu,s} = \rho_0 U_r w_s f_s(r, z) e^{-2i\pi\nu s B/V}. \quad (3.27)$$

Relation (3.27), which will be used in the next chapter, follows easily from Eqs. (3.22) and (3.26).

The parameters needed to evaluate K_c , when solving Eq. (3.25), are listed below:

$$\beta_r: \sqrt{1 - M_r^2},$$

$$\text{Reduced frequency: } K = -sB\Omega b / (\beta_r^2 c_0),$$

$$\text{Inter-vane gap: } h = 2\pi r/V,$$

$$\text{Vane stagger angle: } \alpha_s,$$

$$\Gamma: -\frac{2\pi s B}{V} [1 + M_T M_r(r/r_D) \sin \alpha_s / \beta_r^2].$$

These values appear in the discussion in Appendix A. In the above expressions, M_r is the Mach number for the flow relative to the vanes, and M_T is the rotational Mach number at the rotor blade tip.

CHAPTER 4

DUCT ACOUSTICS

To calculate the duct mode amplitudes excited by the interaction of the stator vanes with the mean rotor wake, we first have to introduce the notion of normal modes. We will then use the loading on the stator vanes from the wakes, in combination with a Green's function integral, to obtain the modal amplitudes. From these modal amplitudes we derive expressions for sound power in the duct.

4.1 Normal Modes in an Annular Duct

The normal modes of an annular duct with hard walls are the set of solutions to the two-dimensional Helmholtz equation having the special form

$$\Psi(r, \phi) = f(r) e^{im\phi}, \quad (4.1)$$

where m is any integer, positive, negative, or zero. The Helmholtz equation is given by

$$\nabla^2 \Psi + \kappa^2 \Psi = 0, \quad (4.2)$$

where ∇^2 is the two-dimensional Laplace operator, in polar coordinates,

$$\nabla^2 \equiv \frac{\partial^2}{\partial r^2} + \frac{1}{r} \frac{\partial}{\partial r} + \frac{1}{r^2} \frac{\partial^2}{\partial \phi^2}. \quad (4.3)$$

In this equation, κ is an undefined constant. As is shown below, the equation has non-trivial solutions which fit the appropriate boundary conditions on the walls of the annular duct only for certain specific values of κ . If Eq. (4.1) is substituted into Eq. (4.2), we obtain

$$\frac{d^2 f}{dr^2} + \frac{1}{r} \frac{df}{dr} + \left(\kappa^2 - \frac{m^2}{r^2} \right) f = 0. \quad (4.4)$$

Substituting $u = \kappa r$ for r reduces Eq. (4.4) to Bessel's equation of order m :

$$\frac{d^2 f}{du^2} + \frac{1}{u} \frac{df}{du} + \left(1 - \frac{m^2}{u^2} \right) f = 0. \quad (4.5)$$

The solutions are m th order Bessel functions of the first and second kind, i.e., $f(u) = \psi_m(\kappa r)$, where

$$\psi_m(\kappa r) = A J_m(\kappa r) + B Y_m(\kappa r). \quad (4.6)$$

If we specify that $\Psi(r, \phi) = \psi_m(\kappa r) \exp(im\phi)$ is either the pressure or the velocity potential, then the radial derivatives of ψ_m must vanish at the inner and outer walls of the duct, so if A and B are to be not both zero,

$$\begin{vmatrix} J'_m(\kappa r_H) & Y'_m(\kappa r_H) \\ J'_m(\kappa r_D) & Y'_m(\kappa r_D) \end{vmatrix} = 0. \quad (4.7)$$

This transcendental equation has a countably infinite number of roots κ for every integer m ; if we denote these roots by κ_{mn} , $n = 1, 2, 3, \dots$, and arrange them in order of increasing magnitude, then the functions $\psi_m(\kappa_{mn} r)$ have $(n - 1)$ zeros in the interval $r_H \leq r \leq r_D$.

These functions are also orthogonal with respect to the weight function r over the same interval; that is,

$$\int_{r_H}^{r_D} r \psi_m(\kappa_{mn} r) \psi_m(\kappa_{m\ell} r) dr = 0 \quad (4.8)$$

unless $\ell = n$. Using this fact, plus the fact that the functions $\exp(im\phi)$, $m = \text{any integer}$, are orthogonal on the interval $0 \leq \phi \leq 2\pi$, it is easy to show that the normal modes $\psi_m(\kappa_{mn} r) \exp(im\phi)$ are orthogonal over the cross-section of the duct. Specifically,

$$\begin{aligned} & \int_{r_H}^{r_D} \int_0^{2\pi} \{\psi_m(\kappa_{mn} r) e^{im\phi}\} \times \{\psi_k(\kappa_{k\ell} r) e^{-ik\phi}\} r d\phi dr \\ &= \begin{cases} 0, & \text{if } k \neq m \text{ or } \ell \neq n; \\ 2\pi \int_{r_H}^{r_D} \psi_m^2(\kappa_{mn} r) r dr, & \text{if } k = m \text{ and } \ell = n. \end{cases} \end{aligned} \quad (4.9)$$

It is convenient to adjust the constants A and B in Eq. (4.6) (which are determined by Eq. (4.7) only to within an arbitrary multiplicative factor) so that

$$\int_{r_H}^{r_D} \psi_m^2(\kappa_{mn} r) r dr = \frac{r_D^2 - r_H^2}{2}. \quad (4.10)$$

The orthogonality relation, i.e., Eq. (4.9), then becomes

$$\int_{r_H}^{r_D} \int_0^{2\pi} \{\psi_m(\kappa_{mn} r) e^{im\phi}\} \times \{\psi_k(\kappa_{kl} r) e^{-ik\phi}\} r d\phi dr = \pi(r_D^2 - r_H^2) \delta_{mk} \delta_{nl}, \quad (4.11)$$

where δ_{mk} and δ_{nl} are Kronecker deltas; δ_{mk} is equal to unity for $m = k$ and equal to zero for $m \neq k$.

A special *FORTTRAN* program has been written which calculates κ_{mn} and the constants A and B in Eq. (4.6) subject to the normalization given in Eq. (4.11); for details see Appendix B.

The significance of the normal modes is that they can be used to represent pressure patterns which propagate within the duct without change in form, and that any acoustic field within the duct, however generated, can be represented as a suitable combination of these patterns.

The wave equation in a duct containing a fluid moving at a uniform axial velocity U is*

$$\nabla^2 p + \frac{\partial^2 p}{\partial x_1^2} - \frac{1}{c_0^2} \left(\frac{\partial}{\partial t} + U \frac{\partial}{\partial x_1} \right)^2 p = 0, \quad (4.12)$$

where p is the acoustic pressure, and ∇^2 is the two-dimensional Laplace operator, defined by expression (4.3).

Now assume that p has the form

$$\psi_m(\kappa_{mn} r) e^{i(m\phi - \gamma x_1 - sB \Omega t)}, \quad (4.13)$$

where we have assumed for frequencies the blade-passing values, $sB\Omega$, introduced in the last chapter. The pressure pattern above has m diametral nodes (like the spokes of a

* Between the rotor and stator an appreciable circumferential velocity exists as well. This velocity is not accounted for in Eq. (4.12).

wheel), and $(n - 1)$ concentric circular nodes. If we substitute expression (4.13) into Eq. (4.12), and recall from Eq. (4.2) that

$$\nabla^2 [\psi_m(\kappa_{mn} r) e^{im\phi}] = -\kappa_{mn}^2 \psi_m(\kappa_{mn} r) e^{im\phi}, \quad (4.14)$$

the following relation is obtained:

$$-\kappa_{mn}^2 - \gamma^2 + \left(\frac{sB\Omega}{c_0} + \frac{U\gamma}{c_0} \right)^2 = 0. \quad (4.15)$$

Solving for γ in terms of κ_{mn} and $sB\Omega$, we set $\gamma = \gamma_{mns}$ and find that

$$\gamma_{mns} = \frac{1}{\beta^2} \left(\frac{MsB\Omega}{c_0} \pm k_{mns} \right), \quad (4.16)$$

where the plus sign is used for upstream propagating waves and the minus sign for downstream ones. Also,

$$k_{mns} = \sqrt{\left(\frac{sB\Omega}{c_0} \right)^2 - \beta^2 \kappa_{mn}^2}. \quad (4.17)$$

In the above expressions, M is the axial flow Mach number, U/c_0 , and $\beta = \sqrt{1 - M^2}$.

Eq. (4.16) shows that γ_{mns} is real whenever $sB\Omega$ is real and $|sB\Omega/c_0| > \beta\kappa_{mn}$. Under these conditions, the pressure pattern propagates unchanged along spiral paths normal to the lines

$$m\phi - \gamma_{mns} x_1 = \text{constant}, \quad (4.18)$$

producing a rotating pattern. If $sB\Omega$ is real but $|sB\Omega/c_0| < \beta\kappa_{mn}$, then γ_{mns} is complex and the pattern grows or decays exponentially along the duct depending on which sign in Eq. (4.16) is selected.

Modal pressure patterns such as

$$\psi_m(\kappa_{mn} r) e^{i(m\phi - \gamma_{mns} x_1 - sB\Omega t)} \quad (4.19)$$

can be superimposed to form a general description of the acoustic pressure field in a turbomachine. Thus, if we multiply the pattern above by an arbitrary coefficient, say p_{mns} , and sum over m, n and s , we obtain

$$p(\vec{x}, t) = \sum_{s=-\infty}^{\infty} \sum_{m=-\infty}^{\infty} \sum_{n=1}^{\infty} p_{mns} \psi_m(\kappa_{mn} r) e^{i(m\phi - \gamma_{mns} x_1 - sB\Omega t)}, \quad (4.20)$$

where now \vec{x} is the point (r, x_1, ϕ) in the duct. Note that in general $p(\vec{x}, t)$ is composed of both propagating and non-propagating modal pressure patterns. The Fourier inverse of this equation gives the sound pressure at the s th harmonic of blade passage frequency:

$$p_s(\vec{x}) = \sum_{m=-\infty}^{\infty} \sum_{n=1}^{\infty} p_{mns} \psi_m(\kappa_{mn} r) e^{i(m\phi - \gamma_{mns} x_1)}. \quad (4.21)$$

It should be noted that, following standard practice, when output is printed in the `V072` code, the radial mode index is adjusted to begin at 0 instead of 1.

4.2 Duct Acoustic Modes

The acoustic modes of the inlet or exhaust ducts were just derived above. In this section, we shall derive equations that relate these modes to fluctuating loads on the stator vanes. The end result will be an expression for the complex pressure amplitudes appearing in Eq. (4.21). If we assume a harmonic time dependence for the excitation, say $f_s(\vec{x}) \exp(-isB\Omega t)$, which is the case for the wake, then pressure at the field point \vec{x} will also be harmonic with the same frequency, and will have the form $p_s(\vec{x}) \exp(-isB\Omega t)$. This is due to the linearity of the governing equations.

It can easily be shown* that the pressure fluctuation $p_s(\vec{x})$ within the duct is given, in terms of the force/unit area $f_s(\vec{x})$ exerted by the vanes on the fluid, by the Green's function integral

$$p_s(\vec{x}) = \int_{S(\vec{y})} \{\nabla_{\vec{y}} G(\vec{x}, \vec{y})\} \cdot \vec{f}_s(\vec{y}) dS(\vec{y}), \quad (4.22)$$

where $S(\vec{y})$ represents both surfaces of the vanes and $\nabla_{\vec{y}}$ is the gradient operator with respect to the vector \vec{y} . In this equation, $G(\vec{x}, \vec{y})$ is the space-only dependent Green's

* One way to see this is to start with Eq. (4.13), the time dependent Green's function integral for density fluctuation $\rho(\vec{x}, t)$, in Ref. 19. Multiply through by c_0^2 to switch to pressure fluctuation $p(\vec{x}, t)$. Then proceed much as is done in section 4.3.2 ("Application to Pure Tones") of Ref. 19 in obtaining Eq. (4.25) there.

function for a hard-walled annular duct. It is the same function as $G_\omega(\vec{y} | \vec{x})$ given by Eq. (1.C.12) in Ref.19. If we introduce a cylindrical coordinate system such that the field point \vec{x} is (r, x_1, ϕ) , while the integration point \vec{y} is (r', y_1, ϕ') , then G can be written as follows

$$G(\vec{x}, \vec{y}) = -\frac{1}{2i} \sum_{m=-\infty}^{\infty} \sum_{n=1}^{\infty} \frac{\psi_m(\kappa_{mn} r) \psi_m(\kappa_{mn} r')}{k_{mns} \Gamma} e^{i[m(\phi-\phi') + \gamma_{mns}(y_1-x_1)]}, \quad (4.23)$$

where $\Gamma = \pi(r_D^2 - r_H^2)$.

The coordinate system used is pictured in Fig. 4.1. This figure is obtained by considering an imaginary cylinder, of radius r , centered at the duct axis of symmetry. The intersection of this surface with the stator is what is depicted. The origin is located where the leading edge of the stator intersects the hub. In contrast to the situation in Fig. 3.1, the origin is always here rather than moving with the leading edge as the radius changes. In expression (4.16), which defines γ_{mns} , the plus sign is used for upstream field points ($x_1 < y_1$) and the minus sign is used for downstream field points.

If the fluid is assumed to be inviscid, the force \vec{f}_s will be normal to the surface,

$$\vec{f}_s = p_s \vec{n}, \quad (4.24)$$

where \vec{n} is the outward surface normal and p_s is the local pressure. Thus

$$p_s(\vec{x}) = \int_{S(\vec{y})} \vec{n}(\vec{y}) \cdot \{\nabla_{\vec{y}} G(\vec{x}, \vec{y})\} p_s(\vec{y}) dS(\vec{y}). \quad (4.25)$$

The integration is to be carried out over both faces of each vane. On each vane, we can divide the integral in the equation above into two parts, one over the forward or upstream face of the vane, and the other over the downstream face. Denoting the upstream face by superscript (+) and the downstream face by superscript (-), we have, because the vanes are very thin,

$$p_s \vec{n} = (p_s^- - p_s^+) \hat{n}, \quad (4.26)$$

where \hat{n} is the unit normal vector erected on the mean surface of the vane as shown in Fig. 4.1. Define Δp_s as $\Delta p_s = p_s^- - p_s^+$, which is positive when the pressure is greater on the lower face of the vane. Then

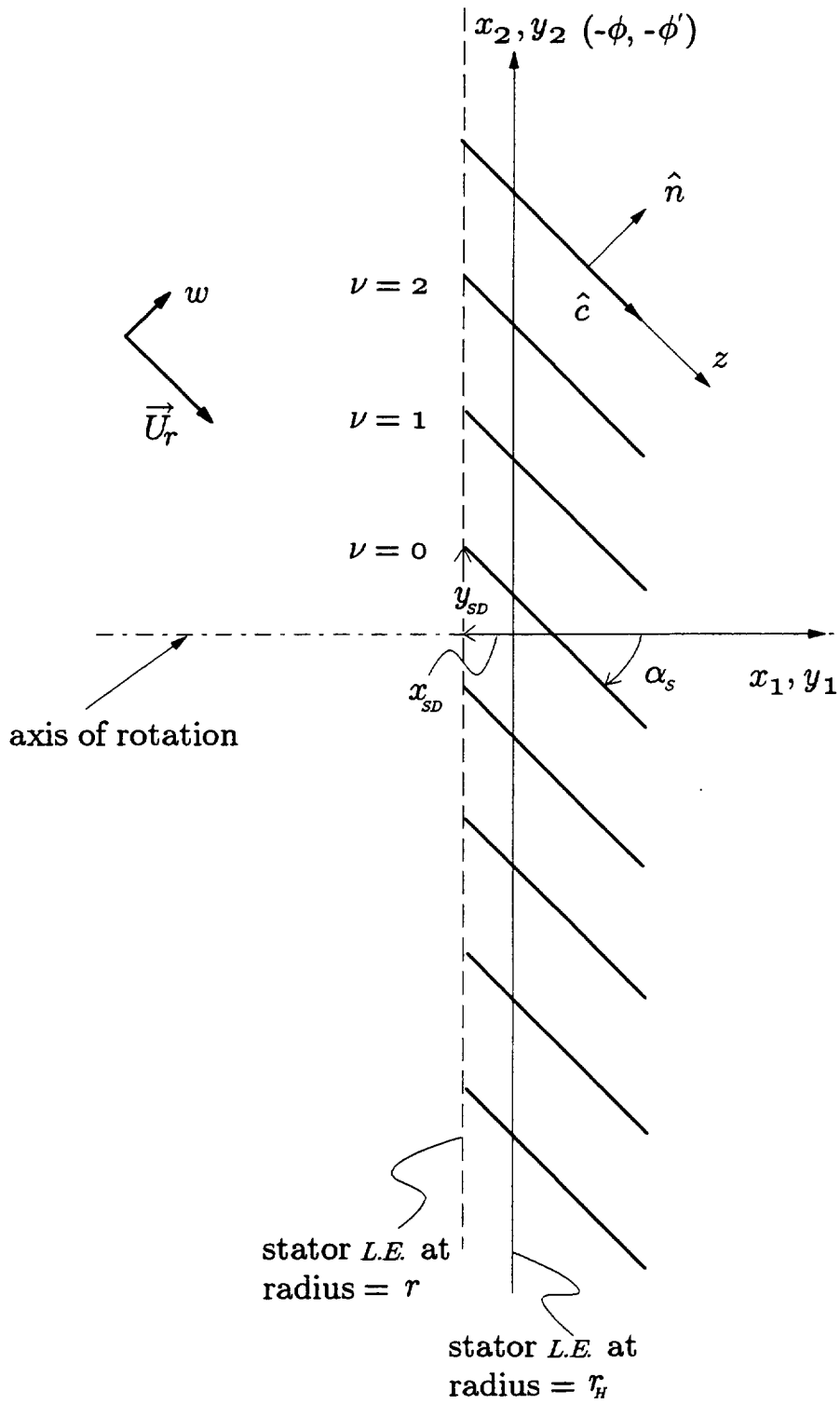


Fig. 4.1 Stator Geometry for Acoustic Mode Analysis.

$$p_s(x) = - \int_{S_M} \hat{n}(\vec{y}) \cdot \{ \nabla_{\vec{y}} G(x, y) \} \Delta p_s(\vec{y}) dS(\vec{y}), \quad (4.27)$$

where now the integration is over the vane mid-surfaces S_M (as opposed to the two vane faces).

Using expression (4.23), Eq. (4.27) can be written as

$$p_s(\vec{x}) = \sum_{m=-\infty}^{\infty} \sum_{n=1}^{\infty} \psi_m(\kappa_{mn} r) e^{i(m\phi - \gamma_{mns} x_1)} \times \frac{1}{2i\Gamma k_{mns}} \int_{S_M} \psi_m(\kappa_{mn} r') \hat{n}(\vec{y}) \cdot \nabla_{\vec{y}} \left[e^{i(-m\phi' + \gamma_{mns} y_1)} \right] \Delta p_s(\vec{y}) dS(\vec{y}). \quad (4.28)$$

Note that $\psi_m(\kappa_{mn} r) \exp[i(m\phi - \gamma_{mns} x_1)]$ is a rotating pressure pattern of the type discussed previously.* Eq. (4.28) is thus a normal mode expansion of the s th harmonic of the acoustic pressure within the duct. Comparing Eqs. (4.21) and (4.28), we see that

$$p_{mns} = \frac{1}{2i\Gamma k_{mns}} \int_{S_M} \psi_m(\kappa_{mn} r') \hat{n}(\vec{y}) \cdot \nabla_{\vec{y}} \left[e^{i(-m\phi' + \gamma_{mns} y_1)} \right] \Delta p_s(\vec{y}) dS(\vec{y}), \quad (4.29)$$

where the p_{mns} are the complex modal amplitudes introduced in Eq. (4.20). Eq. (4.29) is the starting point for evaluating these coefficients.

In Eq. (4.29), the integration is to be carried out over all V stator vanes. As before, to reduce the region of integration to one vane, we arbitrarily select one vane as a reference vane. We assign this vane the number 0, and the remaining vanes, in the direction of decreasing ϕ' , the numbers 0 through $(V - 1)$. Using the notation in Chapter 3, let the pressure on the ν th vane be $\Delta p_{\nu,s}(\vec{y}_0)$, where \vec{y}_0 is the point (r', y_1, ϕ') on the $\nu = 0$ vane. Then the corresponding point on vane ν is $(r', y_1, \phi' - 2\pi\nu/V)$. The total contribution of all V vanes is thus

$$p_{mns} = \frac{1}{2i\Gamma k_{mns}} \int_{S_0} \psi_m(\kappa_{mn} r') \hat{n}(\vec{y}_0) \cdot \nabla_{\vec{y}} \left[e^{i(-m\phi' + \gamma_{mns} y_1)} \right] \times \left\{ \sum_{\nu=0}^{V-1} \Delta p_{\nu,s}(\vec{y}_0) e^{2\pi i m \nu / V} \right\} dS_0(\vec{y}_0), \quad (4.30)$$

* Except for the factor $\exp(-isB\Omega t)$.

where we have gone from a notation where S_M represented the middle surfaces of all the vanes to one where S_0 represents the middle surface of the reference vane.

Referring to the geometry in Fig. 4.1 and noting that the normal vector on the reference vane is $\hat{n} = (\sin \alpha_S, \cos \alpha_S)$, we have that

$$\hat{n} \cdot \nabla_{\vec{y}} \left[e^{i(-m\phi' + \gamma_{mns}y_1)} \right] = i \left(\frac{m}{r'} \cos \alpha_S + \gamma_{mns} \sin \alpha_S \right) e^{i(-m\phi' + \gamma_{mns}y_1)}. \quad (4.31)$$

Note that because ϕ and y_2 are in opposite directions, there is no minus ($-$) sign preceding the m/r' term. To facilitate the integration over the vane surface use the intrinsic chordwise coordinate z' , which as before varies from $-b$ at the leading edge to $+b$ at the trailing edge. From Fig. 4.1 we see that

$$y_1 = -x_{SD} + b \cos \alpha_S + z' \cos \alpha_S, \quad (4.32)$$

$$\phi' = (-y_{SD} + b \sin \alpha_S + z' \sin \alpha_S)/r'. \quad (4.33)$$

Using r' and z' as integration variables, and applying Eqs. (4.31) - (4.33), Eq. (4.30) becomes

$$\begin{aligned} p_{mns} = & \frac{1}{2\Gamma k_{mns}} \int_{r_H}^{r_D} \psi_m(\kappa_{mn} r') \left(\frac{m}{r'} \cos \alpha_S + \gamma_{mns} \sin \alpha_S \right) \\ & \times e^{i(-\gamma_{mns} x_{SD} + m y_{SD}/r')} \int_{-b}^b \left\{ \sum_{\nu=0}^{V-1} \Delta p_{\nu,s}(r', z') e^{2\pi i m \nu / V} \right\} \\ & \times e^{i[(\gamma_{mns} \cos \alpha_S - m \sin \alpha_S / r')(z' + b)]} dz' dr'. \end{aligned} \quad (4.34)$$

The s th harmonic of the pressure loading on vane ν is given by Eq. (3.27). If we substitute this into Eq. (4.34), we have

$$\begin{aligned}
p_{mns} &= \frac{\rho_0}{2\Gamma k_{mns}} \int_{r_H}^{r_D} \psi_m(\kappa_{mn} r') U_r w_s \left(\frac{m}{r'} \cos \alpha_S + \gamma_{mns} \sin \alpha_S \right) \\
&\quad \times e^{i(-\gamma_{mns} x_{SD} + m y_{SD}/r')} \left\{ \sum_{\nu=0}^{V-1} e^{2\pi i \nu (m-sB)/V} \right\} \\
&\quad \times \int_{-b}^b f_s(r', z') e^{i[(\gamma_{mns} \cos \alpha_S - m \sin \alpha_S / r') (z'+b)]} dz' dr'.
\end{aligned} \tag{4.35}$$

The sum over vane number in Eq. (4.35) can be evaluated explicitly:

$$\sum_{\nu=0}^{V-1} e^{2\pi i \nu (m-sB)/V} = \begin{cases} V, & \text{if } m - sB = -qV; \\ 0, & \text{otherwise.} \end{cases}$$

Here q is any integer. The final result is

$$\begin{aligned}
p_{mns} &= \frac{\rho_0 V}{2\Gamma k_{mns}} \int_{r_H}^{r_D} \psi_m(\kappa_{mn} r) U_r w_s(r) \left(\frac{m}{r} \cos \alpha_S + \gamma_{mns} \sin \alpha_S \right) \\
&\quad \times e^{i(-\gamma_{mns} x_{SD} + m y_{SD}/r)} \int_{-b}^b f_s(r, z) e^{i[(\gamma_{mns} \cos \alpha_S - m \sin \alpha_S / r)(z+b)]} dz dr,
\end{aligned} \tag{4.36}$$

where now the primes have been dropped from z and r , and the index m is given by

$$m = sB - qV. \tag{4.37}$$

Eq. (4.36) is our final result. As is evident from Eq. (4.36) above, p_{mns} is proportional to w_s , the s th-order Fourier coefficient of the mean rotor wake. The computer code computes these coefficients, as mentioned previously, using semi-empirical information. However, the code can easily be modified to accept the Fourier coefficients of the wake velocity as inputs, and compute the duct modes directly from them. Additionally, new semi-empirical wake modules could be added to V072 to supplement those already there.

As a final remark, let us note that once the pressure amplitudes, p_{mns} , are specified by virtue of Eq. (4.36), the pressure at any point within the duct can also be determined, if desired, from the summation

$$p(\vec{x}, t) = \sum_{q=-\infty}^{\infty} \sum_{n=1}^{\infty} \sum_{s=-\infty}^{\infty} p_{mns} \psi_{mns}(\kappa_{mns} r) e^{i(m\phi - \gamma_{mns} x_1 - sB\Omega t)}, \quad (4.38)$$

where $m = sB - qV$.

4.3 Sound Power

The flux of sound power in the duct, is found by substituting Eq. (4.36) into Eq. (C.20) of Appendix C, which is written as

$$\text{Power} = \frac{\pi(r_D^2 - r_H^2)}{\rho_0 U} \sum_{q=-\infty}^{\infty} \sum_{n=1}^{\infty} \sum_{s=-\infty}^{\infty} G_{mns} |p_{mns}|^2. \quad (4.39)$$

Here G_{mns} is defined as

$$G_{mns} = \frac{\mp M^2 \beta^4 (sB\Omega/U) k_{mns}}{(sB\Omega/c_0 \pm Mk_{mns})^2}. \quad (4.40)$$

The upper set of signs apply upstream of the stator and the lower set apply downstream. The details describing how power is determined are presented in Appendix C. In Eq. (4.39), the index m is given by Eq. (4.37). Finally, if the sound power at one specific harmonic of the blade passage frequency is desired, the summation over s is deleted, and s is set equal to the desired harmonic number.

Note that for a propagating mode (m, n) at harmonic s , another mode $(-m, n)$ of complex conjugate amplitude propagates with frequency $-s$. Because the amplitudes are complex conjugates, *v072* only calculates positive harmonics. The total sound power for the mode is then evaluated from just the one by applying a factor of 2.

CHAPTER 5

NON-DIMENSIONAL RESULTS

The *V072* program uses non-dimensional input geometry and performance parameters. It uses these quantities to compute dimensionless versions of pressure amplitudes and power and then converts the results to dimensional values. The final output of the program is the magnitude and phase of each propagating mode excited by the interaction of the stator vanes with the wake of the rotor. The sound power flux per mode is also computed and, by summing over all propagating modes, the total sound power flux is obtained. Note that propagating modes are those discussed in Section 4.1 for which $sB\Omega/c_0 > \beta\kappa_{mn}$. Modes for which $sB\Omega/c_0 < \beta\kappa_{mn}$ are said to be cut off and are not included in the output. Note also that a multi-vaned stator, as seen by Eq. (4.37), excites only a subset of the propagating modes at any given frequency; specifically, only modes whose number of diametral nodes, m , is related to the number of rotor blades and stator vanes by the equation $m = sB - qV$, where s and q are arbitrary integers. The program takes this selection mechanism into account in choosing which mode amplitudes to compute.

In performing its calculations, *V072* is divided into two parts. It first carries out the rotor wake calculations and then computes the acoustic results. To do this, it needs both geometric and performance input. Note that performance data would normally come from a steady aerodynamic prediction code of axisymmetric or two-dimensional nature. (See Ref. 3 for more discussion of this.)

Non-dimensionalization in *V072* is with respect to a reference pressure $\frac{1}{2}\rho_0 U^2$, a reference power $\frac{1}{8}\rho_0 c_0^3 M^4 r_D^2$, lengths r_D and b_T , and speeds c_0, U and U_r . Here ρ_0 is the nominal flow density, U the mean axial fluid velocity, c_0 the speed of sound in the duct, $M = U/c_0$, r_D the duct outer radius, and b_T the vane semi-chord at the tip.

5.1 Pressure Amplitude

The dimensionless expression for the complex pressure amplitudes is easily derived starting from Eq. (4.36). After straightforward effort, it takes the form

$$\frac{p_{mns}}{\frac{1}{2}\rho_0 U^2} = \frac{\sigma_c V}{\pi(1-\sigma_r^2)\tilde{k}_{mns}} \int_{\sigma_r}^1 \left(\frac{U_r}{U}\right)^2 \tilde{w}_s \psi_m(X_{mn}x) \left(\frac{m}{x} \cos \alpha_s + \tilde{\gamma}_{mns} \sin \alpha_s\right) \times e^{i[(-\tilde{\gamma}_{mns}x_s + m y_s/x)\sigma_c]} \tilde{b} C_{mns}(x) dx. \quad (5.1)$$

In the above, $\sigma_c = 2b_T/r_D$; $\sigma_r = r_H/r_D$ where r_H is the hub radius; $\tilde{\gamma}_{mns} = \gamma_{mns} r_D$, where γ_{mns} , the axial wave number, is the same as in Eq. (4.16); and $\tilde{k}_{mns} = k_{mns} r_D$ where k_{mns} is the same as in Eq. (4.17). Note that $\tilde{\gamma}_{mns}$ and \tilde{k}_{mns} can be written, explicitly, as

$$\tilde{\gamma}_{mns} = \frac{1}{\beta^2} (sBMM_T) \pm \tilde{k}_{mns} \quad (5.2)$$

and

$$\tilde{k}_{mns} = \sqrt{(sBMM_T)^2 - \beta^2 X_{mn}^2}, \quad (5.3)$$

where M_T is the rotor rotational Mach number at the blade tip and $\beta = \sqrt{1 - M^2}$. Further, in Eq. (5.1), $X_{mn} = \kappa_{mn} r_D$ where κ_{mn} is the eigenvalue for mode (m, n) ; $x = r/r_D$; $x_s = x_{sD}/2b_T$; $y_s = y_{sD}/2b_T$; and $\tilde{b} = b/2b_T$.

Additionally, $C_{mns}(x)$ is the same chordwise integral of the elemental blade loading function f_s^* multiplied by an exponential function, as seen in Eq. (4.36), only here non-dimensionalized using the chordwise parameter z/b . It is given by the expression

$$C_{mns}(x) = \int_{-b}^b f_s e^{i[\sigma_c \tilde{b}(\tilde{\gamma}_{mns} \cos \alpha_s - m \sin \alpha_s/x)(1+z/b)]} \frac{dz}{b}. \quad (5.4)$$

Because f_s has a square root singularity at the leading edge ($z/b = -1$), it is necessary to change the integration variable from z/b to ψ , where $z/b = \cos \psi$. We then have

$$C_{mns}(x) = \int_0^\pi f_s \sin \psi e^{i[\sigma_c \tilde{b}(\tilde{\gamma}_{mns} \cos \alpha_s - m \sin \alpha_s/x)(1+\cos \psi)]} d\psi. \quad (5.5)$$

This integral is easy to compute numerically using Simpson's rule, because the product $f_s \sin \psi$ is finite at the leading edge ($\psi = \pi$).

* Note that the elemental loading function f_s becomes a different function as its independent variable changes from step to step. However, for simplicity of notation, we still denote it as f_s .

The parameter \tilde{w}_s , used in Eq. (5.1), is defined as w_s/U_r , where w_s is the quantity given by Eq. (3.20) and U_r is given by Eq. (3.9). It can be written as

$$\begin{aligned} \tilde{w}_s = \check{w}_s e^{-isB[\sigma_c(y_R+y_S)/x - x_{SOR} \tan \alpha_{CL} + x_{SOR,H} \tan \alpha_{CL,H}]} \\ \times e^{-isB[\sigma_c \bar{b}(\sin \alpha_S + \cos \alpha_S \tan \alpha_{CL})/x]}, \end{aligned} \quad (5.6)$$

where

$$\check{w}_s = \frac{W_s}{U_r} \sin(\alpha_S + \alpha_{CL}). \quad (5.7)$$

Also, $y_R = y_{RD}/2b_T$ and $x_{SOR} = x_{SPAC}/2b_T$.

The spanwise integration in Eq. (5.1) requires special treatment because \tilde{w}_s , as seen in Eq. (5.6), contains a phase angle, $x_{SOR} \tan \alpha_{CL}$, which varies rapidly over the span when the separation between rotor and stator is large or when the relative flow angle at the stator leading edge, α_{CL} , is a strong function of the radius, r . To handle this rapidly varying phase, an adaptation of Filon's rule of integration has been used for the spanwise integration (see Appendix D). Note also that for spanwise integration, V072 requires values of geometric and performance quantities at radial locations determined internally by the program. To obtain these parameters at the necessary locations, V072 linearly interpolates the pertinent input data.

To obtain $f_s(y/b)$, which is needed in Eq. (5.4) to evaluate $C_{mn_s}(x)$, one solves the dimensionless version of Eq. (3.25) which is easily seen to take the form

$$e^{i\tilde{k}_s z/b} = \int_{y/b=-1}^1 K_c\left(\frac{z-y}{b}\right) f_s\left(\frac{y}{b}\right) d\left(\frac{y}{b}\right), \quad (5.8)$$

whose kernel function $K_c((z-y)/b)$, as mentioned previously, is derived in Appendix A. The quantity \tilde{k}_s is the non-dimensional version of the vane chordwise wavenumber k_s (see expression (3.19)). It is given by

$$\tilde{k}_s = k_s b = \frac{sB\sigma_c \bar{b}}{x} (\sin \alpha_S + \cos \alpha_S \tan \alpha_{CL}). \quad (5.9)$$

Finally, there are issues as regards a singularity at the leading edge. For this reason Eq. (5.8) must be changed to the form

$$e^{i\tilde{k}_s \cos \theta} = \int_0^\pi K_c(\cos \theta - \cos \psi) F_s(\psi) d\psi, \quad (5.10)$$

using the same chordwise type transformations as used previously, i.e., $z/b = \cos \theta$ and $y/b = \cos \psi$. In Eq. (5.10) we then have $F_s(\psi) = f_s(\cos \psi) \sin \psi$. The singularity issues along with a solution of Eq. (5.10) using the method of collocation (Refs. 20 and 21) are discussed in Appendix E.

Note that, in the code, magnitudes and phases of the pressure mode amplitudes are printed out. The phases are given for positive values of the index s . The magnitudes are r.m.s. values obtained by time-averaging the square of the sum of the $+s$ and $-s$ waves, $\{p_{mns} \exp(-isB\Omega t) + p_{(-m)n(-s)} \exp(isB\Omega t)\}^2$. Since $p_{(-m)n(-s)} = p_{mns}^*$, the result of this calculation is $\sqrt{2} |p_{mns}|$. Before output, the magnitudes are converted back to dimensional form through multiplication by $\frac{1}{2}\rho_0 U^2$. The final result is then presented in dB units relative to a reference pressure of $0.0002 \times 1.4504 \times 10^{-4}$ psi (i.e., 2×10^{-5} Pa).

5.2 Sound Power

Given the modal amplitudes $p_{mns}/(\frac{1}{2}\rho_0 U^2)$, the sound power is obtained from Eq. (4.39). Non-dimensionalizing by $\frac{1}{8}\rho_0 c_0^3 M^4 r_D^2$, we have

$$\frac{\text{Power}}{\frac{1}{8}\rho_0 c_0^3 M^4 r_D^2} = \sum_{q=-\infty}^{\infty} \sum_{n=1}^{\infty} \frac{2\pi(r_D^2 - r_H^2) G_{mns}}{M r_D^2} \left| \frac{p_{mns}}{\frac{1}{2}\rho_0 U^2} \right|^2, \quad (5.11)$$

where G_{mns} is the quantity given by Eq. (4.40), $m = sB - qV$, and sound power in Eq. (5.11) is for one specific harmonic, s , of the blade passage frequency. In obtaining Eq. (5.11), we have used the fact that $\frac{1}{8}\rho_0 c_0^3 M^4 r_D^2$ is equivalent to $\frac{1}{8}\rho_0 U^3 M r_D^2$. Eq. (5.11) can finally be re-written as

$$\frac{\text{Power}}{\frac{1}{8}\rho_0 c_0^3 M^4 r_D^2} = \sum_{q=-\infty}^{\infty} \sum_{n=1}^{\infty} 2\pi (1 - \sigma_r^2) \tilde{G}_{mns} \left| \frac{p_{mns}}{\frac{1}{2}\rho_0 U^2} \right|^2, \quad (5.12)$$

where

$$\tilde{G}_{mns} = \frac{\mp \tilde{k}_{mns} s B M_T \beta^4}{(s B M_T \pm M \tilde{k}_{mns})^2}. \quad (5.13)$$

Again, as for expression (4.40), the upper set of signs apply to power for waves propagating upstream and the lower set apply downstream.

V072 gives values of sound power for three different cases: (1) for the sum of all modes with a given s ; (2) for the sum of all modes with a given s and m ; and (3) for individual modes with given s , m , and n . Case (1) is treated using Eq. (5.12); case (2) using Eq. (5.12) with the summation over q deleted and q set to give the value of m desired; and case (3) by taking the individual term in Eq. (5.12) corresponding to m, n, s . For all three cases, as for the mode amplitudes, the actual power output comes from summing the values for both $+s$ and $-s$. Additionally, the power is converted back to dimensional form, through multiplication by $\frac{1}{8}\rho_0 c_0^3 M^4 r_D^2$, and then given in dB units relative to a reference power of $10^{-12}/1.3558$ ft-lbs/sec (10^{-12} watts).

CHAPTER 6

CONCLUDING REMARKS

This report is an updated version of the analytical documentation for the *V072 Rotor Wake/Stator Interaction Code*. It provides updated geometry and revised equations and has eliminated the material related to turbulent acoustic sources, because these sources are not active in the code. Additionally, equations are now developed in terms of integer multiples of blade passage frequency, rather than the more general frequency ω used when turbulence was covered.

In this report, equations have been derived for the amplitudes and power of the propagating duct modes excited by a turbofan (rotor/stator stage) operating at subsonic tip speed within an infinite hard-walled annular duct. The equations used in the code are non-dimensional and the output is tone noise generated by the mean velocity defect wakes of the rotor blades impinging on the stator vanes. Output is provided at blade passage frequencies for the propagating (cut on) modes.

APPENDIX A

KERNEL FUNCTION FOR A LINEAR CASCADE IN SUBSONIC FLOW

The kernel function for a cascade of thin airfoils in oscillating subsonic flow has been derived by several investigators, using a variety of methods (Refs. 5-9, 22). Of the various approaches employed to date, the method of Fourier transforms is perhaps the most straightforward. This procedure was used in Ref. 9, for example, but the inversion of the Fourier transform was accomplished numerically. More recently, Goldstein (Ref. 19) pointed out that the Fourier transform of the kernel function contains no branch points, so the inversion can be accomplished quite easily by using the Cauchy residue theorem. Goldstein outlined the procedure to be followed, but did not actually carry out the calculation of the kernel function. The purpose of this appendix is to set forth the details of the inversion, and to record the end result. For the convenience of the reader, as well as to document the notation used, a brief derivation of the transform of the kernel function is also presented.

The cascade geometry is shown in Fig. A.1. The airfoil semi-chord is b , and the gap between the neighboring airfoils is bh , with components bh_1 , projected along the chord, and bh_2 , normal to it. The airfoils are shown as having no camber, because the ultimate objective is to calculate the pressure field scattered by the cascade when it is subjected to vorticity convected with the mean flow. However, other situations, such as a cascade of oscillating airfoils, can be handled as well. For the purpose of calculating the kernel function, we need only suppose that a known chordwise pressure distribution exists on each airfoil, and calculate the resulting velocity field.

The first step is to calculate the upwash generated by a single airfoil. Let the pressure be given by the real part of $p \exp(-isB\Omega t)$, and the corresponding velocity field be the real part of $(w_1, w_2) \exp(-isB\Omega t)$. Then, p satisfies the convected wave equation, and the velocity field is related to the gradient of p through the equations of motion.* These equations are

* p and (w_1, w_2) now represent the s th harmonics of pressure and velocity field.

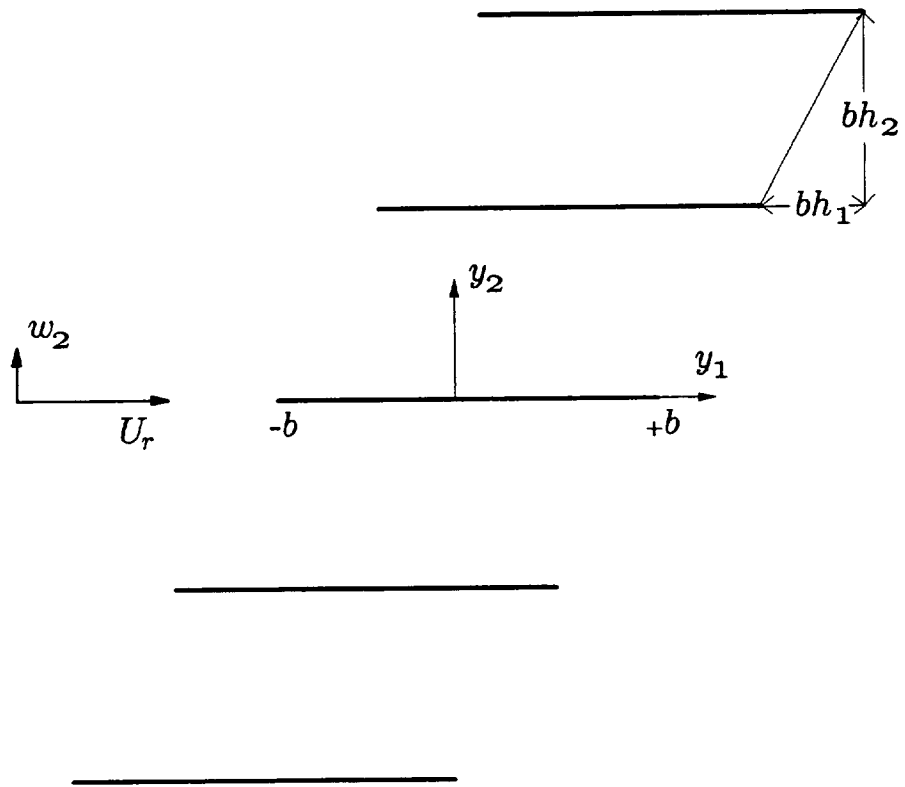


Fig. A.1 Stator Cascade Geometry.

$$\frac{\partial^2 p}{\partial y_1^2} + \frac{\partial^2 p}{\partial y_2^2} - \frac{1}{c_0^2} \left(-isB\Omega + U_r \frac{\partial}{\partial y_1} \right)^2 p = 0, \quad (\text{A.1})$$

$$\left(-isB\Omega + U_r \frac{\partial}{\partial y_1} \right) w_j + \frac{1}{\rho_0} \frac{\partial p}{\partial y_j} = 0; \quad j = 1, 2. \quad (\text{A.2})$$

Consistent with the definition of Fourier series in Chapter 3, the following definition of the Fourier transform pair is chosen:

$$p = \frac{1}{2\pi} \int_{-\infty}^{+\infty} \bar{p} e^{i\alpha y_1} d\alpha, \quad (\text{A.3})$$

$$\bar{p} = \int_{-\infty}^{+\infty} p e^{-i\alpha y_1} dy_1. \quad (\text{A.4})$$

The Fourier transforms of Eq. (A.1) and the second of Eqs. (A.2), i.e., for $j = 2$ are

$$\frac{d^2 \bar{p}}{dy_2^2} - \lambda^2 \bar{p} = 0, \quad (\text{A.5})$$

$$i(-sB\Omega + \alpha U_r) \bar{w}_2 + \frac{1}{\rho_0} \frac{d\bar{p}}{dy_2} = 0, \quad (\text{A.6})$$

where

$$\lambda = [\alpha^2 - M_r^2(\alpha - sB\Omega/U_r)^2]^{\frac{1}{2}}. \quad (\text{A.7})$$

The pressure p generated by an isolated airfoil is bounded at infinity, and, because the airfoils are assumed to have zero thickness, is antisymmetric in y_2 . A solution of Eq. (A.5) satisfying these conditions is

$$\bar{p} = -\frac{\Delta \bar{p}(\alpha)}{2} e^{-\lambda |y_2|} \text{sgn}(y_2), \quad (\text{A.8})$$

provided that λ is defined so that its real part is non-negative on the path of integration used to invert the Fourier transform. In Eq. (A.8), $\Delta \bar{p}(\alpha)$ is the Fourier transform of the chordwise pressure distribution, Δp , on the airfoil. (Δp is positive if the pressure is greatest on the lower face of the airfoil.) By eliminating \bar{p} between Eqs. (A.6) and (A.8),

we obtain the Fourier transform of the upwash generated by a single airfoil. The upwash itself is

$$\frac{w_2}{U_r}(y_1, y_2) = -\frac{1}{2\pi} \int_{-\infty}^{+\infty} \frac{\lambda}{2i(\alpha - sB\Omega/U_r)} \frac{\Delta\bar{p}(\alpha)}{\rho_0 U_r^2} e^{i\alpha y_1 - \lambda|y_2|} d\alpha. \quad (\text{A.9})$$

The upwash generated by a cascade of airfoils, located at the points $(y_1, y_2) = m(bh_1, bh_2)$, $m = 0, \pm 1, \pm 2, \dots$, is obtained by summing the contributions of the individual airfoils:

$$\begin{aligned} \frac{w_2}{U_r}(y_1, y_2) = & -\frac{1}{2\pi} \sum_{m=-\infty}^{+\infty} \int_{-\infty}^{+\infty} \frac{\lambda}{2i(\alpha - sB\Omega/U_r)} \frac{\Delta\bar{p}_m(\alpha)}{\rho_0 U_r^2} \\ & \times e^{i\alpha(y_1 - mbh_1) - \lambda|y_2 - mbh_2|} d\alpha. \end{aligned} \quad (\text{A.10})$$

This infinite series can be summed analytically if the transformed pressure distributions on successive airfoils in the cascade [i.e., $\Delta\bar{p}_m(\alpha)$] are related by a constant increment in phase angle. That is, for any integer m ,

$$\Delta\bar{p}_m(\alpha) = \Delta\bar{p}_0(\alpha) e^{im\sigma}, \quad (\text{A.11})$$

where $\Delta\bar{p}_0(\alpha)$ is the transform of the pressure on the “zeroth” (i.e., reference) airfoil, and σ (called the inter-blade phase angle) is a constant given by*

$$\sigma = -\frac{2\pi sB}{V}. \quad (\text{A.12})$$

To calculate the upwash near any selected vane, say vane ν , introduce

$$x_1 = y_1 - \nu bh_1, \quad (\text{A.13})$$

$$x_2 = y_2 - \nu bh_2, \quad (\text{A.14})$$

and

$$n = m - \nu. \quad (\text{A.15})$$

* This value can be derived by proceeding as in Ref. 23, page 38, only using our definitions of geometry and parameters.

Then

$$\begin{aligned} \frac{w_2}{U_r}(x_1 + \nu bh_1, x_2 + \nu bh_2) = \\ - \frac{e^{i\nu\sigma}}{2\pi} \int_{-\infty}^{+\infty} \frac{\Delta \bar{p}_0(\alpha)}{\rho_0 U_r^2} \frac{\lambda S(\alpha) e^{i\alpha x_1}}{2i(\alpha - sB\Omega/U_r)} d\alpha, \end{aligned} \quad (\text{A.16})$$

where the infinite series

$$S(\alpha) = \sum_{n=-\infty}^{+\infty} e^{(i\nu\sigma - \lambda|x_2 - nbh_1| - i\alpha nbh_2)}, \quad (\text{A.17})$$

can be summed as

$$S(\alpha) = \frac{1}{2} \left[\frac{e^{(\frac{1}{2}\Delta_+ - \lambda x_2)}}{\sinh(\frac{1}{2}\Delta_+)} - \frac{e^{(\frac{1}{2}\Delta_- + \lambda x_2)}}{\sinh(\frac{1}{2}\Delta_-)} \right], \quad (\text{A.18})$$

for

$$0 \leq x_2 < bh_2, \quad (\text{A.19})$$

where

$$\Delta_{\pm} = \pm \lambda bh_2 + i(\sigma - \alpha bh_1). \quad (\text{A.20})$$

Now, use the convolution theorem to calculate the inverse of Eq. (A.16)

$$\frac{w_2}{U_r}(x_1 + \nu bh_1, x_2 + \nu bh_2) = e^{i\nu\sigma} \int_{-b}^{+b} K_c(x_1 - \zeta, x_2) \frac{\Delta p_0(\zeta)}{\rho_0 U_r^2} \frac{d\zeta}{b}, \quad (\text{A.21})$$

where K_c is the desired cascade kernel function given by

$$K_c(x_1, x_2) = - \frac{b}{2\pi} \int_{-\infty}^{+\infty} \frac{\lambda S e^{i\alpha x_1}}{2i(\alpha - sB\Omega/U_r)} d\alpha. \quad (\text{A.22})$$

The factor b is included to make K_c dimensionless.

It is convenient to introduce dimensionless variables, as follows:

$$\begin{aligned}
K &= -sB\Omega b/(\beta_r^2 c_0), & \check{x}_1 &= x_1/b, \\
\check{\alpha} &= \alpha b - M_r K, & \check{x}_2 &= x_2/b.
\end{aligned}
\tag{A.23}$$

where β_r was defined at the end of Chapter 3. The shifted transform variable $\check{\alpha}$ completes the squares in λ :

$$\lambda = \frac{\beta_r}{b} \sqrt{\check{\alpha}^2 - K^2}.$$
(A.24)

Then

$$K_c = -\frac{\beta_r e^{iKM_r \check{x}_1}}{2\pi i} \int_{-\infty}^{+\infty} \frac{\gamma S e^{i\check{\alpha}\check{x}_1}}{2(\check{\alpha} + K/M_r)} d\check{\alpha},$$
(A.25)

where now

$$\gamma = (\check{\alpha}^2 - K^2)^{\frac{1}{2}},$$
(A.26)

$$S = \frac{1}{2} \left[\frac{e^{(\frac{1}{2}\Delta_+ - \beta_r \gamma \check{x}_2)}}{\sinh(\frac{1}{2}\Delta_+)} - \frac{e^{(\frac{1}{2}\Delta_- + \beta_r \gamma \check{x}_2)}}{\sinh(\frac{1}{2}\Delta_-)} \right].$$
(A.27)

Notice that γS is an even function of γ , so that even though the integrand contains the variable

$$\gamma = \sqrt{\check{\alpha}^2 - K^2},$$
(A.28)

there can be no branch points at $\check{\alpha} = \pm K$. Thus, if we apply the residue theorem to evaluate the kernel function by closing the path of integration on a large arc in the upper or lower $\check{\alpha}$ -plane, no residual integrals around branch cuts appear; the kernel function is simply the sum of the residues in the upper or lower half plane. To insure that the integrals on the arcs vanish as their radii are allowed to become infinitely large, the integrand in Eq. (A.25) must be modified. First, note that

$$S = \frac{1}{(\beta_r \gamma)^2} \frac{\partial^2 S}{\partial \check{x}_2^2}$$
(A.29)

so K_c can be written as follows

$$K_c = -\frac{e^{iKM_r\check{x}_1}}{2\pi i\beta_r} \frac{\partial^2}{\partial\check{x}_2^2} \int_{-\infty}^{+\infty} \frac{Se^{i\check{\alpha}\check{x}_1}}{2\gamma(\check{\alpha} + K/M_r)} d\check{\alpha}. \quad (\text{A.30})$$

The integral above can be evaluated via the residue theorem by using the contours shown in Fig. A.2, and the differentiation with respect to \check{x}_2 carried out afterwards. If $\check{x}_1 > 0$, the integral around the semicircle in the upper half plane vanishes when the radius of the contour goes to infinity. Thus,

$$K_c = -\frac{1}{\beta_r} e^{iKM_r\check{x}_1} \frac{\partial^2}{\partial\check{x}_2^2} \left\{ \begin{array}{l} \text{sum of residues in} \\ \text{upper half plane} \end{array} \right\}. \quad (\text{A.31})$$

On the other hand, when $\check{x}_1 < 0$ the integral around the contour in the lower half plane vanishes, so

$$K_c = +\frac{1}{\beta_r} e^{iKM_r\check{x}_1} \frac{\partial^2}{\partial\check{x}_2^2} \left\{ \begin{array}{l} \text{sum of residues in} \\ \text{lower half plane} \end{array} \right\}. \quad (\text{A.32})$$

The integrand in Eq. (A.30) has poles at $\check{\alpha} = -K/M_r$, and at points where $\sinh(\frac{1}{2}\Delta_{\pm}) = 0$. The latter set of points are located at α_n^{\pm} where

$$\Delta_{\pm} = 2n\pi i \quad (n = \text{any integer}) \quad (\text{A.33})$$

[cf. Eq. (A.27)]. When Δ_{\pm} is real, some of these poles lie directly on the real axis. To arrive at the correct expression for K_c , it is necessary to invoke the causality condition by stipulating that K has a small negative imaginary part. Once the kernel function has been evaluated, we can let $\text{Im}(K) \rightarrow 0$. The effect of this procedure is to eliminate the possibility that acoustic waves not generated by the cascade itself are inadvertently included in the solution.

If $\text{Im}(K) < 0$, the pole at $\check{\alpha} = -K/M_r$ is clearly in the upper half plane. The residue

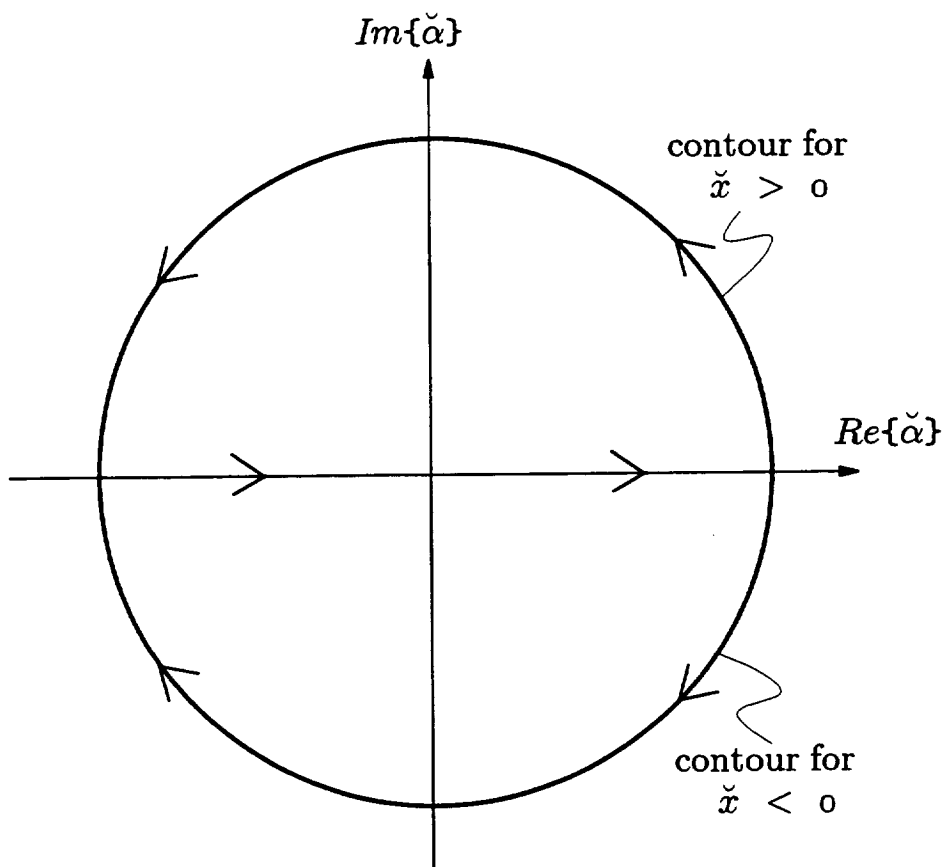


Fig. A.2 Integration Contour for Eq. (A.30).

is

$$R_K = \frac{M_r}{2\beta_r K} \left[\frac{\sinh(\beta_r^2 K h_2 / M_r)}{\cosh(\beta_r^2 K h_2 / M_r) - \cos(\Gamma + K h_1 / M_r)} \right] e^{-iK\check{x}_1 / M_r}, \quad (\text{A.34})$$

where

$$\Gamma = \sigma - \alpha b h_1 - \frac{K h_1}{M_r}. \quad (\text{A.35})$$

Using Eq. (A.12) for σ , Eq. (A.23c) to obtain α when $\check{\alpha} = -K/M_r$, and Eq. (A.23a) for K , we can rewrite Eq. (A.35) as

$$\Gamma = -\frac{2\pi s B}{V} \left[1 + M_r M_r (r/r_D) \sin \alpha_s / \beta_r^2 \right], \quad (\text{A.36})$$

which is the expression for Γ used in the code.

The roots α_n^\pm of Eq. (A.33) are given by

$$\alpha_n^\pm = \frac{\Gamma_n h_1}{d^2} \pm \frac{\beta_r h_2}{d} \left[K^2 - (\Gamma_n / d)^2 \right]^{\frac{1}{2}}, \quad (\text{A.37})$$

where

$$\Gamma_n = \Gamma - 2n\pi, \quad (\text{A.38})$$

$$d = \sqrt{h_1^2 + \beta_r^2 h_2^2}. \quad (\text{A.39})$$

If the square root in Eq. (A.37) is defined as follows,

$$[Re^{i\theta}]^{\frac{1}{2}} = \sqrt{R} e^{i\theta/2}, \quad 0 \leq \theta < 2\pi, \quad (\text{A.40})$$

where \sqrt{R} is the positive square root of R , then solutions α_n^\pm having the plus (minus) sign in Eq. (A.37) are located in the upper (lower) half plane. In either case, the residue is

$$R_n(\alpha_n^\pm) = \frac{\beta_r h_2}{2d^2} \left[\frac{1}{(\alpha_n^\pm - \Gamma_n h_1 / d^2) (\alpha_n^\pm + K / M_r)} \right] e^{i\alpha_n^\pm \check{x}_1}. \quad (\text{A.41})$$

Using Eqs. (A.31) and (A.32), and carrying out the indicated differentiations, we

obtain the final result

$$\begin{aligned}
K_c = & \frac{\beta_r^2 K}{2M_r} \left[\frac{\sinh(\beta_r^2 K h_2 / M_r)}{\cosh(\beta_r^2 K h_2 / M_r) - \cos(\Gamma + K h_1 / M_r)} \right] e^{-i\beta_r^2 K \check{x}_1 / M_r} \\
& - \frac{\beta_r^2 h_2}{2d^2} \sum_{n=-\infty}^{+\infty} \left[\frac{(\alpha_n^{+2} - K^2)}{(\alpha_n^+ - \Gamma_n h_1 / d^2) (\alpha_n^+ + K / M_r)} \right] e^{i(\alpha_n^+ + K M_r) \check{x}_1}
\end{aligned} \tag{A.42}$$

if $\check{x}_1 > 0$, and

$$K_c = \frac{\beta_r^2 h_2}{2d^2} \sum_{n=-\infty}^{+\infty} \left[\frac{(\alpha_n^{-2} - K^2)}{(\alpha_n^- - \Gamma_n h_1 / d^2) (\alpha_n^- + K / M_r)} \right] e^{i(\alpha_n^- + K M_r) \check{x}_1} \tag{A.43}$$

if $\check{x}_1 < 0$. Having calculated the kernel function for $\text{Im}(K) < 0$, we can now let $\text{Im}(K) \rightarrow 0$. Then the roots α_n^\pm become, using the branch of the square root employed previously in Eq. (A.37)

$$\alpha_n^\pm = \frac{\Gamma_n h_1}{d^2} \pm i \frac{\beta_r h_2}{d} \sqrt{(\Gamma_n / d)^2 - K^2} \tag{A.44}$$

if $|\Gamma_n / d| > K$, and

$$\alpha_n^\pm = \frac{\Gamma_n h_1}{d^2} \mp \frac{\beta_r h_2}{d} \sqrt{K^2 - (\Gamma_n / d)^2} \tag{A.45}$$

if $|\Gamma_n / d| < K$. In Eqs. (A.44) and (A.45), α_n^+ is to be calculated using the upper set of signs, and α_n^- using the lower set of signs. The $\sqrt{\quad}$ sign means the positive square root.

APPENDIX B

NUMERICAL COMPUTATION OF THE NORMAL MODES IN AN ANNULAR DUCT

As discussed in Chapter 4, the normal modes in an annular duct are functions of the form

$$\psi_m(\kappa_{mn} r) = AJ_m(\kappa_{mn} r) + BY_m(\kappa_{mn} r), \quad (\text{B.1})$$

where $J_m(\cdot)$ and $Y_m(\cdot)$ are Bessel functions of the first and second kinds, and κ_{mn} 's are the roots of the following transcendental equation:

$$\begin{vmatrix} J'_m(\kappa r_H) & Y'_m(\kappa r_H) \\ J'_m(\kappa r_D) & Y'_m(\kappa r_D) \end{vmatrix} = 0. \quad (\text{B.2})$$

The roots $\kappa_{mn} r_D$ of Eq. (B.1) are found by first estimating the roots as follows:

$$\kappa_{mn} r_D \doteq \begin{cases} m, & \text{if } n = 1; \\ \kappa_{m, n-1} r_D + \pi, & \text{if } n > 1. \end{cases} \quad (\text{B.3})$$

This estimate is refined by incrementing the estimated value of $\kappa_{mn} r_D$ by $\pi/10$ until the determinant in Eq. (B.2) changes sign. The step size is then halved and changed in sign. This process continues until the absolute value of the determinant is reduced to a preassigned value. In the code, this is done utilizing the non-dimensional versions of the above equations.

Once the eigenvalue κ_{mn} has been computed, the constants A and B are assigned one of the following two sets of values:

$$\begin{cases} A = 1 \\ B = -\frac{J'_m(\kappa_{mn} r_D)}{Y'_m(\kappa_{mn} r_D)} \end{cases} \quad \text{or} \quad \begin{cases} A = -\frac{Y'_m(\kappa_{mn} r_D)}{J'_m(\kappa_{mn} r_D)} \\ B = 1 \end{cases}. \quad (\text{B.4})$$

Of these two sets of values, the one for which $(A^2 + B^2)$ is the smaller value is chosen. If $(A^2 + B^2)$ is the same for both, then the second set is picked. The desired normalization, namely,

$$\int_{r_H}^{r_D} \psi_m^2(\kappa_{mn} r) r dr = \frac{1}{2}(r_D^2 - r_H^2), \quad (\text{B.5})$$

is obtained by computing the value of the integral on the left-hand side of the equation above, using the formula

$$\int_{r_H}^{r_D} \psi_m^2(\kappa_{mn} r) r dr = \frac{1}{2} \left(r^2 - \frac{m^2}{\kappa_{mn}^2} \right) \psi_m^2(\kappa_{mn} r) \Big|_{r=r_H}^{r_D} \equiv C. \quad (\text{B.6})$$

The constants A and B are then divided by

$$\sqrt{2C/(r_D^2 - r_H^2)} \quad (\text{B.7})$$

to give the normalization required by Eq. (B.5).

Note that in terms of non-dimensional variables, Eqs. (B.5) and (B.6) can be written, respectively, as

$$\int_{\sigma_r}^1 \psi_m^2(X_{mn} x) x dx = \frac{1}{2}(1 - \sigma_r^2) \quad (\text{B.8})$$

and

$$\int_{\sigma_r}^1 \psi_m^2(X_{mn} x) x dx = \frac{1}{2} \left(x^2 - \frac{m^2}{X_{mn}^2} \right) \psi_m^2(X_{mn} x) \Big|_{x=\sigma_r}^1. \quad (\text{B.9})$$

The non-dimensional parameters in Eqs. (B.8) and (B.9) are the same as the ones originally used in Chapter 5. It is easily seen that the factor by which A and B are to be divided, can be written explicitly as

$$\sqrt{\frac{(1 - m^2/X_{mn}^2)\psi_m^2(X_{mn}) - (\sigma_r^2 - m^2/X_{mn}^2)\psi_m^2(X_{mn} \sigma_r)}{1 - \sigma_r^2}}. \quad (\text{B.10})$$

APPENDIX C

SOUND POWER FLUX

The sound power flux through any cross-section of the duct is given by (Ref. 19)

$$\text{Power} = \int_{A_D} \langle I_{ax} \rangle dA, \quad (\text{C.1})$$

where I_{ax} is the axial component of the acoustic energy flux vector, $\langle I_{ax} \rangle$ is the acoustic intensity, which is defined as

$$\langle I_{ax} \rangle = \frac{B\Omega}{2\pi} \int_{-\pi/B\Omega}^{\pi/B\Omega} I_{ax} dt, \quad (\text{C.2})$$

and A_D is the cross-sectional area of the duct. In a duct containing a fluid flowing at a uniform axial velocity U , I_{ax} is, in turn, given by

$$I_{ax} = \left(\frac{p}{\rho_0} + Uu \right) (\rho_0 u + \rho U), \quad (\text{C.3})$$

where ρ_0 is the nominal fluid density and p , ρ , and u are the instantaneous acoustic perturbation pressure, density and axial velocity, respectively. The quantities p and u are real. Although not explicitly stated, all acoustic variables are functions of both space and time.

The acoustic pressure and density perturbations are proportional to one another ($p = c_0^2 \rho$), so Eq. (C.3) can be rewritten in terms of the pressure and axial velocity as

$$I_{ax} = (1 + M^2) pu + \frac{M}{\rho_0 c_0} pp + \rho_0 c_0 M uu, \quad (\text{C.4})$$

where $M = U/c_0$ is the nominal axial flow Mach number. For p and u real, we can write $pu = pu^*$ and $uu = uu^*$, where the superscript $*$ denote the complex conjugate. Hence, Eq. (C.4) can be rewritten as

$$I_{ax} = (1 + M^2) pu^* + \frac{M}{\rho_0 c_0} pp^* + \rho_0 c_0 M uu^*. \quad (\text{C.5})$$

For functions of t , we reverse the Fourier series sign convention used in Eqs. (3.5) and (3.6) for the spatial variables. Then, p can be written as the Fourier series

$$p(\vec{x}, t) = \sum_{s=-\infty}^{\infty} p_s(\vec{x}) e^{-isB\Omega t}, \quad (\text{C.6})$$

where

$$p_s(\vec{x}) = \frac{B\Omega}{2\pi} \int_{-\pi/B\Omega}^{\pi/B\Omega} p(\vec{x}, t) e^{isB\Omega t} dt. \quad (\text{C.7})$$

There is a corresponding definition for $u(\vec{x}, t)$ and $u_s(\vec{x})$. The axial acoustic energy flux, I_{ax} , can now be written as a double summation

$$I_{ax} = \sum_{s=-\infty}^{\infty} \sum_{\mu=-\infty}^{\infty} \left[(1 + M^2) p_s(\vec{x}) u_{\mu}^*(\vec{x}) + \frac{M}{\rho_0 c_0} p_s(\vec{x}) p_{\mu}^*(\vec{x}) + \rho_0 c_0 M u_s(\vec{x}) u_{\mu}^*(\vec{x}) \right] e^{-i(s-\mu)B\Omega t}. \quad (\text{C.8})$$

Both $p_s(\vec{x})$ and $u_{\mu}(\vec{x})$ can be written as sums of modal pressure patterns as in Eq. (4.21). Thus

$$p_s(\vec{x}) = \sum_{m=-\infty}^{\infty} \sum_{n=1}^{\infty} p_{mns} \psi_m(\kappa_{mn} r) e^{i(m\phi - \gamma_{mns} x_1)}, \quad (\text{C.9})$$

$$u_{\mu}(\vec{x}) = \sum_{k=-\infty}^{\infty} \sum_{\ell=1}^{\infty} u_{k\ell\mu} \psi_k(\kappa_{k\ell} r) e^{i(k\phi - \gamma_{k\ell\mu} x_1)}. \quad (\text{C.10})$$

The modal coefficients p_{mns} and u_{mns} are not independent, but are related through the axial momentum equation,

$$\frac{\partial u}{\partial t} + U \frac{\partial u}{\partial x_1} + \frac{1}{\rho_0} \frac{\partial p}{\partial x_1} = 0. \quad (\text{C.11})$$

Let the pressure and axial velocity be given, for each harmonic, by the real parts, respectively, of $p_s \exp(-isB\Omega t)$ and $u_s \exp(-isB\Omega t)$. Then Eq. (C.11) reduces to

$$-isB\Omega u_s + U \frac{\partial u_s}{\partial x_1} + \frac{1}{\rho_0} \frac{\partial p_s}{\partial x_1} = 0. \quad (\text{C.12})$$

If Eqs. (C.9) and (C.10) are substituted in Eq. (C.12), the following relationship is obtained,

$$u_{mns} = -\frac{A_{mns}}{\rho_0 U} p_{mns}, \quad (\text{C.13})$$

where

$$A_{mns} = \frac{\gamma_{mns}}{sB\Omega/U + \gamma_{mns}}. \quad (\text{C.14})$$

The axial acoustic energy flux can now be written entirely in terms of p_{mns} :

$$\begin{aligned} I_{ax} = & \sum_{m=-\infty}^{\infty} \sum_{n=1}^{\infty} \sum_{k=-\infty}^{\infty} \sum_{\ell=1}^{\infty} \psi_m(\kappa_{mn} r) \psi_k(\kappa_{k\ell} r) e^{i(m-k)\phi} \\ & \times \frac{1}{\rho_0 U} \sum_{s=-\infty}^{\infty} \sum_{\mu=-\infty}^{\infty} [M^2 - (1 + M^2) A_{k\ell\mu}^* + A_{mns} A_{k\ell\mu}^*] \\ & \times e^{-i[(\gamma_{mns} - \gamma_{k\ell\mu})x_1 - (s-\mu)B\Omega t]} p_{mns} p_{k\ell\mu}^*. \end{aligned} \quad (\text{C.15})$$

Using this relation and Eq. (C.2), then

$$\begin{aligned} \langle I_{ax} \rangle = & \sum_{m=-\infty}^{\infty} \sum_{n=1}^{\infty} \sum_{k=-\infty}^{\infty} \sum_{\ell=1}^{\infty} \psi_m(\kappa_{mn} r) \psi_k(\kappa_{k\ell} r) e^{i(m-k)\phi} \\ & \times \frac{B\Omega}{2\pi\rho_0 U} \sum_{s=-\infty}^{\infty} \sum_{\mu=-\infty}^{\infty} \int_{-\pi/B\Omega}^{\pi/B\Omega} [M^2 - (1 + M^2) A_{k\ell\mu}^* + A_{mns} A_{k\ell\mu}^*] \\ & \times e^{-i[(\gamma_{mns} - \gamma_{k\ell\mu})x_1 - (s-\mu)B\Omega t]} p_{mns} p_{k\ell\mu}^* dt = \\ & \sum_{m=-\infty}^{\infty} \sum_{n=1}^{\infty} \sum_{k=-\infty}^{\infty} \sum_{\ell=1}^{\infty} \psi_m(\kappa_{mn} r) \psi_k(\kappa_{k\ell} r) e^{i(m-k)\phi} \\ & \times \frac{1}{\rho_0 U} [M^2 - (1 + M^2) A_{k\ell s}^* + A_{mns} A_{k\ell s}^*] \\ & \times e^{-i(\gamma_{mns} - \gamma_{k\ell s})x_1} p_{mns} p_{k\ell s}^*. \end{aligned} \quad (\text{C.16})$$

Note that in obtaining Eq. (C.16), those terms in the integrand for which $\mu \neq s$, are periodic in t over the interval $2\pi/B\Omega$, and thus they average out to zero and do not contribute to the integral.

Substituting for $\langle I_{ax} \rangle$ in Eq. (C.1), the sound power is found by performing the integration over the cross-section of the duct. Utilizing the orthogonality conditions that exist, to eliminate product terms involving different modes, we find that

$$\begin{aligned} \text{Power} &= \int_0^{2\pi} \int_{r_H}^{r_D} \langle I_{ax} \rangle r dr d\phi = \frac{\pi(r_D^2 - r_H^2)}{\rho_0 U} \\ &\times \sum_{m=-\infty}^{\infty} \sum_{n=1}^{\infty} \sum_{s=-\infty}^{\infty} [M^2 - (1 + M^2) A_{mns}^* + |A_{mns}|^2] |p_{mns}|^2, \end{aligned} \quad (\text{C.17})$$

where the integral over the cross-sectional area of the duct A_p is written explicitly in terms of r and ϕ coordinates.

The term in the square brackets which, henceforth, we denote as G_{mns} , can be simplified, resulting in

$$G_{mns} = \frac{\mp M^2 \beta^4 (sB\Omega/U) k_{mns}}{[sB\Omega/c_0 \pm M k_{mns}]^2}, \quad (\text{C.18})$$

where the upper set of signs applies upstream of the stator and the lower set applies downstream. In terms of G_{mns} , then, we have

$$\text{Power} = \frac{\pi(r_D^2 - r_H^2)}{\rho_0 U} \sum_{m=-\infty}^{\infty} \sum_{n=1}^{\infty} \sum_{s=-\infty}^{\infty} G_{mns} |p_{mns}|^2. \quad (\text{C.19})$$

Finally, recalling that the index m is related to the summation indices s and q through the relation $m = sB - qV$, Eq. (C.19) becomes

$$\text{Power} = \frac{\pi(r_D^2 - r_H^2)}{\rho_0 U} \sum_{q=-\infty}^{\infty} \sum_{n=1}^{\infty} \sum_{s=-\infty}^{\infty} G_{mns} |p_{mns}|^2. \quad (\text{C.20})$$

APPENDIX D

FILON'S INTEGRATION RULE

Filon's integration rule applies to integrals of the form

$$\int_a^b f(x)e^{ig(x)} dx, \quad (\text{D.1})$$

where the phase function $g(x)$ is a "large" linear function of x , so that use of the trapezoidal rule or Simpson's rule would require that the interval of integration be divided into many subintervals to obtain an accurate answer. Filon's rule is obtained by assuming that the function $f(x)$ can be approximated by a quadratic function, but the exponential function $\exp[ig(x)]$ is integrated exactly. To extend this procedure to integrals wherein $g(x)$ is not a linear function of x , we need only approximate it as a linear function within each x subinterval. The most straightforward procedure is to approximate both $f(x)$ and $g(x)$ as linear functions of x . For example, to compute the following integral

$$I = \int_a^b f(x) e^{ig(x)} dx, \quad (\text{D.2})$$

divide the interval (a, b) into N equal subintervals of length $h = (b - a)/N$. The integral over the n th subinterval is then

$$I_n = \int_{x_n}^{x_n+h} f(x) e^{ig(x)} dx. \quad (\text{D.3})$$

To compute this integral, approximate both $f(x)$ and $g(x)$ as linear functions:

$$f(x) = f_n + (f_{n+1} - f_n) \left(\frac{x - x_n}{h} \right), \quad (\text{D.4})$$

$$g(x) = g_n + (g_{n+1} - g_n) \left(\frac{x - x_n}{h} \right), \quad (\text{D.5})$$

where $f_n = f(x_n)$, and so on. Carrying out the integrations, we obtain

$$I_n = h(a^* f_n + a f_{n+1}) e^{i g_0}, \quad (\text{D.6})$$

where

$$g_0 = \frac{1}{2}(g_n + g_{n+1}), \quad (\text{D.7})$$

$$\lambda = \frac{1}{2}(g_n - g_{n+1}), \quad (\text{D.8})$$

$$a = \frac{\sin \lambda}{2\lambda} + i \left(\frac{\sin \lambda}{2\lambda^2} - \frac{\cos \lambda}{2\lambda} \right), \quad (\text{D.9})$$

and a^* is the complex conjugate of a . When $\lambda \rightarrow 0$, the integral over the n th subinterval becomes

$$I_n = \frac{h}{2}(f_n + f_{n+1}), \quad (\text{D.10})$$

which is the trapezoidal rule.

If an even number of subintervals are used, it is also possible to approximate $f(x)$ as a quadratic function (over any two neighboring subintervals) while leaving $g(x)$ as a linear function of x . This integration scheme reduces to Simpson's rule when $g(x)$ is constant. Both the trapezoidal and the quadratic versions of Filon's rule have been tried. Because the quadratic version did not seem to improve the convergence significantly over the simpler trapezoidal rule, the latter scheme is used in the *V072* program.

APPENDIX E

NUMERICAL SOLUTION OF THE INTEGRAL EQUATION FOR THE BLADE LOADING

As discussed in Chapter 5, the elemental blade loading function $f_s(y/b)$ is the solution of Eq. (5.8), which with subscript s suppressed in this appendix, becomes

$$e^{i\bar{k}z/b} = \int_{y/b=-1}^1 K_c\left(\frac{z-y}{b}\right) f\left(\frac{y}{b}\right) d\left(\frac{y}{b}\right). \quad (\text{E.1})$$

This integral equation contains two basic difficulties. They are:

- (a) the solution $f(z/b)$ has a singularity of the type $(z+b)^{-\frac{1}{2}}$ at the leading edge ($z = -b$), and
- (b) the kernel function $K_c(y/b)$ contains both a Cauchy singularity ($1/y$) and a logarithmic singularity at $y = 0$.

Difficulty (a) is circumvented by introducing the chordwise transformations $z/b = \cos \theta$ and $y/b = \cos \psi$. Equation (E.1) then becomes

$$e^{i\bar{k} \cos \theta} = \int_0^\pi K_c(\cos \theta - \cos \psi) F(\psi) d\psi, \quad (\text{E.2})$$

where $F(\psi) = f(\cos \psi) \sin \psi$. Whereas $f(\cos \psi)$ is singular at $\psi = \pi$, $F(\psi)$ is not. Thus the integral equation is solved for F rather than for f itself. Difficulty (b) is overcome by special treatment of the logarithmically singular part of the kernel.

To solve Eq. (E.2), we apply the method of collocation. That is, the integral on the right-hand side of Eq. (E.2) is required to equal the forcing function on the left-hand side at the N points

$$\theta_m = (m - 1/2)\pi; \quad m = 1, \dots, N. \quad (\text{E.3})$$

The equations to be solved are then

$$e^{i\bar{k} \cos \theta_m} = I(\theta_m); \quad m = 1, \dots, N, \quad (\text{E.4})$$

where

$$I(\theta) = \int_0^{\pi} K_c(\cos \theta - \cos \psi) F(\psi) d\psi. \quad (\text{E.5})$$

In computing $I(\theta)$ by evaluating the right-hand side of Eq. (E.5), the points

$$\psi_\ell = \ell\pi/N, \quad \ell = 0, 1, \dots, N, \quad (\text{E.6})$$

are used.* Having the collocation and integration points interlaced has the dual effect of avoiding the point $\psi = \theta$, where K_c is singular, and of ensuring that the solution obtained satisfies the Kutta condition, which requires that $F = 0$ at the trailing edge.

The logarithmic portion of the kernel function must be isolated for special treatment.

Thus,

$$K_c(y/b) = K_1(y/b) + G(y/b) \log |y/b| \quad (\text{E.7})$$

and

$$I(\theta) = I_1(\theta) + I_L(\theta), \quad (\text{E.8})$$

where

$$I_1(\theta) = \int_0^{\pi} K_1(\cos \theta - \cos \psi) F(\psi) d\psi, \quad (\text{E.9})$$

$$I_L(\theta) = \int_0^{\pi} G(\cos \theta - \cos \psi) \log |\cos \theta - \cos \psi| F(\psi) d\psi. \quad (\text{E.10})$$

The trapezoidal rule suffices to compute $I_1(\theta)$,

$$I_1(\theta) = \sum_{\ell=0}^N \frac{\pi}{N} B_\ell K_1(\cos \theta - \cos \psi_\ell) F(\psi_\ell), \quad (\text{E.11})$$

* Because $F(0) = 0$, use of $N + 1$ integration points as called for in Eq. (E.6) introduces only N unknowns $F(\ell\pi/N)$, for $\ell = 1, \dots, N$.

where $B_0 = B_N = 1/2$, while $B_\ell = 1$ otherwise; but a special integration rule, devised by Whitehead (Refs. 20, 21) is required for the logarithmic portion of the kernel. Whitehead's integration rule is given as

$$I_L(\theta) = \sum_{\ell=0}^N \frac{\pi}{N} B_\ell G(\cos \theta - \cos \psi_\ell) \log |\cos \theta - \cos \psi| S_\ell(\theta), \quad (\text{E.12})$$

where the B_ℓ 's are the same weighting functions as defined above, and

$$S_\ell(\theta) = - \left\{ \log 2 + 2 \sum_{s=1}^N \frac{1}{s} B_s \cos(s\theta) \cos(s\ell\pi/N) \right\}. \quad (\text{E.13})$$

Note that because of the comment in the footnote on page 57, the summations in Eqs. (E.11) and (E.12) actually begin at $\ell = 1$ rather than $\ell = 0$. Hence by combining $I_1(\theta)$ and $I_L(\theta)$, the integral equation is reduced to the following set of algebraic equations for the unknowns $F(\ell\pi/N)$,

$$e^{i\bar{k} \cos\{(m-1/2)\pi/N\}} = \sum_{\ell=1}^N A_{m\ell} F(\ell\pi/N), \quad m = 1, \dots, N, \quad (\text{E.14})$$

where

$$A_{m\ell} = \frac{\pi}{N} B_\ell \left\{ K_c(x) + G(x) [S_\ell(\theta_m) - \log |x|] \right\} \quad (\text{E.15})$$

and

$$x = \cos(\theta_m) - \cos(\psi_\ell). \quad (\text{E.16})$$

Any standard matrix package which handles equations with complex coefficients can be used to solve these equations.

REFERENCES

1. Ventres, C.S., M.A. Theobald, and W.D. Mark, "Turbofan Noise Generation, Volume 1: Analysis," NASA CR-167951, July 1982.
2. Ventres, C.S., M.A. Theobald, and W.D. Mark, "Turbofan Noise Generation, Volume 2: Computer Programs," NASA CR-167952, July 1982.
3. Topol, D.A. and D.C. Mathews, "Rotor Wake/Stator Interaction Noise Prediction Code, Technical and User's Manual," NASA Contract No. NAS3-25952 (Task 10) Report, October 1992.
4. Danda Roy, I., W. Eversman, and H.D. Meyer, "Improved Finite Element Modeling of the Turbofan Engine Inlet Radiation Problem," NASA Contract No. NAS3-25952 (Task 10) Report, April 1993.
5. Kemp, N.H. and W.R. Sears, "Aerodynamic Interference between Moving Blade Rows," *Journal of Aeronautical Sciences*, 20, 9, 1953, pp. 585-597.
6. Kemp, N.H. and W.R. Sears, "The Unsteady Forces due to Viscous Wakes in Turbomachines," *Journal of Aeronautical Sciences*, 22, 7, 1955, pp. 478-483.
7. Fleeter, S., "Fluctuating Lift and Moment Coefficients for Cascaded Airfoils in a Nonuniform Compressible Flow," *Journal of Aircraft*, 10, 2, 1973, pp. 93-98.
8. Kaji, S., "Noncompact Source Effect on the Prediction of Tone Noise from a Fan Rotor," AIAA Paper 75-446, March 1975.
9. Kobayashi, H., "Three Dimensional Effects on Pure Tone Fan Noise due to Inflow Distortion," AIAA Paper 78-1120, July 1978.
10. Kobayashi, H. and J.F. Groeneweg, "Effects of Inflow Distortion Profiles on Fan Tone Noise," *AIAA Journal*, Vol. 18, No. 8, August 1980, pp. 899-906.
11. Namba, M., "Three-Dimensional Analysis of Blade Force and Sound Generation for an Annular Cascade in Distorted Flows," *Journal of Sound and Vibration*, Vol. 50, February 1977, pp. 479-508.

12. Namba, M., "Lifting Surface Theory for a Rotating Subsonic or Transonic Blade Row," Aeronautical Research Council, Reports and Memoranda No. 3740, 1974.
13. Reynolds, B., B. Lakshminarayana, and A. Ravindranath, "Characteristics of the Near Wake of a Compressor or Fan Rotor Blade," *AIAA Journal*, Vol. 17, No. 9, September 1979, pp. 959-967.
14. Reynolds, B. and B. Lakshminarayana, "Characteristics of Lightly Loaded Fan Rotor Blade Wakes," NASA CR-3188, October 1979.
15. Ravindranath, A. and B. Lakshminarayana, "Three Dimensional Mean Flow and Turbulence Characteristics of the Near Wake of a Compressor Rotor Blade," NASA CR-159518, June 1980.
16. Majjigi, R.K. and P.R. Gliche, "Development of a Rotor Wake/Vortex Model, Volume 1: Final Report," NASA CR-174849, June 1984.
17. Topol, D.A. and D.A. Philbrick, "Fan Noise Prediction System Development: Wake Model Improvements and Code Evaluations," NASA Contract No. NAS3-25952 (Task 10) Report, April 1993.
18. Bliss, D.B., K.L. Chandiramani, and A.G. Piersol, "Data Analysis and Noise Prediction for the QF-1B Experimental Fan Stage," NASA CR-135066, August 1976.
19. Goldstein, M.E., *Aeroacoustics*, McGraw-Hill, New York, 1976.
20. Whitehead, D.S., "Force and Moment Coefficients for Vibrating Aerofoils in Cascade," Aeronautical Research Council Reports and Memoranda, No. 3254, February 1960.
21. Smith, S.N., "Discrete Frequency Sound Generation in Axial Flow Turbomachines," Aeronautical Research Council Reports and Memoranda, No. 3709, March 1972.
22. Mark, W.D., "Characterization of Rotor Inlet Turbulence for Rotor Noise Predictions," Bolt Beranek & Newman Inc. Technical Memorandum, No. 486, December 1978.
23. Hanson, D.B., "Coupled 2-Dimensional Cascade Theory for Noise and Unsteady Aerodynamics of Blade Row Interaction in Turbofans, Vol. 1 - Theory Development and Parametric Studies," NASA CR-4506, January 1994.

ACKNOWLEDGEMENTS

The authors would like to thank Donald B. Hanson and David A. Topol of Pratt & Whitney, R.M. Nallasamy of NYMA, Inc., and Edward J. Rice of E.J. Rice Consulting for their helpful critiques and suggestions. Additionally, we thank Donald B. Hanson, along with Dennis L. Huff and John F. Groeneweg of NASA Lewis Research Center, for originally suggesting this project and for their support.

Acknowledgement should also go to the authors of the original *V072* documentation, C.S. Ventres, M.A. Theobald and W.D. Mark, from whose report we borrowed, intact, much of the material used herein.

REPORT DOCUMENTATION PAGE

Form Approved
OMB No. 0704-0188

Public reporting burden for this collection of information is estimated to average 1 hour per response, including the time for reviewing instructions, searching existing data sources, gathering and maintaining the data needed, and completing and reviewing the collection of information. Send comments regarding this burden estimate or any other aspect of this collection of information, including suggestions for reducing this burden, to Washington Headquarters Services, Directorate for Information Operations and Reports, 1215 Jefferson Davis Highway, Suite 1204, Arlington, VA 22202-4302, and to the Office of Management and Budget, Paperwork Reduction Project (0704-0188), Washington, DC 20503.

1. AGENCY USE ONLY (Leave blank)	2. REPORT DATE March 1996	3. REPORT TYPE AND DATES COVERED Final Contractor Report	
4. TITLE AND SUBTITLE Aeroacoustic Analysis of Turbofan Noise Generation		5. FUNDING NUMBERS WU-538-03-11 C-NAS3-26618 C-NAS3-27186	
6. AUTHOR(S) Harold D. Meyer and Edmane Envia		8. PERFORMING ORGANIZATION REPORT NUMBER E-10148	
7. PERFORMING ORGANIZATION NAME(S) AND ADDRESS(ES) United Technologies Corporation Hamilton Standard Division Windsor Locks, Connecticut 06096		10. SPONSORING/MONITORING AGENCY REPORT NUMBER NASA CR-4715	
9. SPONSORING/MONITORING AGENCY NAME(S) AND ADDRESS(ES) National Aeronautics and Space Administration Lewis Research Center Cleveland, Ohio 44135-3191		11. SUPPLEMENTARY NOTES Harold D. Meyer, United Technologies Corporation, Hamilton Standard Division, Windsor Locks, Connecticut 06096 (work funded by NASA Contract NAS3-26618) and Edmane Envia, NYMA, Inc., 2001 Aerospace Parkway, Brook Park, Ohio 44142 (work funded by NASA Contract NAS3-27186). Project Manager, Dennis L. Huff, Propulsion Systems Division, NASA Lewis Research Center, organization code 2770, (216) 433-3913.	
12a. DISTRIBUTION/AVAILABILITY STATEMENT Unclassified - Unlimited Subject Categories 07 and 71 This publication is available from the NASA Center for Aerospace Information, (301) 621-0390.		12b. DISTRIBUTION CODE	
13. ABSTRACT (Maximum 200 words) This report provides an updated version of analytical documentation for the <i>V072 Rotor Wake/Stator Interaction Code</i> . It presents the theoretical derivation of the equations used in the code and, where necessary, it documents the enhancements and changes made to the original code since its first release. <i>V072</i> is a package of <i>FORTRAN</i> computer programs which calculate the in-duct acoustic modes excited by a fan/stator stage operating in a subsonic mean flow. Sound is generated by the stator vanes interacting with the mean wakes of the rotor blades. In this updated version, only the tonal noise produced at the blade passing frequency and its harmonics, is described. The broadband noise component analysis, which was part of the original report, is not included here. The code provides outputs of modal pressure and power amplitudes generated by the rotor-wake/stator interaction. The rotor/stator stage is modeled as an ensemble of blades and vanes of zero camber and thickness enclosed within an infinite hard-walled annular duct. The amplitude of each propagating mode is computed and summed to obtain the harmonics of sound power flux within the duct for both upstream and downstream propagating modes.			
14. SUBJECT TERMS Rotor/stator interaction; Rotor wake; Fan noise generation; Cascade; Source noise modeling; Duct acoustics		15. NUMBER OF PAGES 73	
17. SECURITY CLASSIFICATION OF REPORT Unclassified		16. PRICE CODE A04	
18. SECURITY CLASSIFICATION OF THIS PAGE Unclassified	19. SECURITY CLASSIFICATION OF ABSTRACT Unclassified	20. LIMITATION OF ABSTRACT	



**National Aeronautics and
Space Administration**

Lewis Research Center
21000 Brookpark Rd.
Cleveland, OH 44135-3191

Official Business
Penalty for Private Use \$300

POSTMASTER: If Undeliverable — Do Not Return